

# Application of the ECT9 protocol for radiocarbon-based source apportionment of carbonaceous aerosols

Lin Huang<sup>1\*</sup>, Wendy Zhang<sup>1</sup>, Guaciara M. Santos<sup>2</sup>, Blanca T. Rodríguez<sup>2</sup>, Sandra R. Holden<sup>2</sup>, Vincent Vetro<sup>1</sup>, Claudia I. Czimczik<sup>2\*</sup>

5 <sup>1</sup>Climate Research Division, Atmospheric Science & Technology Directorate, Environment and Climate Change Canada, Toronto, ON M3H 5T4, Canada

<sup>2</sup>Department of Earth System Science, University of California, Irvine, CA 92697-3100, USA

\*Correspondence to: Lin Huang ([lin.huang@canada.ca](mailto:lin.huang@canada.ca)); Claudia I. Czimczik ([czimczik@uci.edu](mailto:czimczik@uci.edu))

Key words: Radiocarbon, organic carbon, elemental carbon, black carbon, Arctic, EnCan-total-900, SRM1649a

10 **Abstract:** Carbonaceous aerosol is mainly composed of organic carbon (OC) and elemental carbon (EC). Both OC and EC originate from a variety of emission sources. Radiocarbon ( $^{14}\text{C}$ ) analysis can be used to apportion bulk aerosol, OC, and EC into their sources. However, such analyses require the physical separation of OC and EC.

15 Here, we apply of ECT9 protocol to physically isolate OC and EC for  $^{14}\text{C}$  analysis and evaluate its effectiveness. Several reference materials are selected, including: two pure OC (fossil “adipic acid”, contemporary “sucrose”), two pure EC (fossil “regal black” and “C1150”), and three complex materials containing contemporary and/or fossil OC and EC (“rice char” and NIST urban dust standards “SRM1649a”, i.e., bulk dust and “SRM8785”, i.e., fine fraction of re-suspended SRM1649a on filter). The pure materials were measured for their OC, EC and total carbon (TC) mass fractions and corresponding carbon isotopes to evaluate the uncertainty of the procedure. The average accuracy of TC mass, determined via volumetric injection of a sucrose solution, was approximately 5%. Ratios of EC/TC and OC/TC were highly reproducible, with analytical 20 precisions better than 2% for all reference materials, ranging in size from 20 to 100  $\mu\text{g C}$ . Consensus values were reached for all pure reference materials for both  $\delta^{13}\text{C}$  and fraction modern  $\text{FM}^{14}\text{C}$  with an uncertainty of <0.3‰ and approximately 5% Commented [CC1]: Consider replacing with “F”

25 respectively. The procedure introduced 1.3±0.6  $\mu\text{g}$  of extraneous carbon, an amount compatible to that of the Swiss\_4S protocol.

30 In addition, OC and EC were isolated from mixtures of pure contemporary OC (sucrose) with pure fossil EC (regal black) and fossil OC (adipic acid) with contemporary EC (rice char EC) to evaluate the effectiveness of OC and EC separation. Consensus  $\text{FM}^{14}\text{C}$  values were reached for all OC (~5-30  $\mu\text{g}$ ) and EC (~10-60  $\mu\text{g}$ ) fractions with an uncertainty of <5%. We found that the ECT9 protocol efficiently isolates OC or EC from complex mixtures. Based on  $\delta^{13}\text{C}$  measurements, the average contribution of charred OC to EC is likely less than 3% when the OC loading amount is less than 30  $\mu\text{g C}$ .

35 Charring was further assessed by evaluating thermograms of various materials, including aerosol samples collected in the Arctic and from tailpipes of gasoline or diesel engines. These data demonstrate that the ECT9 method effectively removes pyrolyzed OC. Thus, the ECT9 protocol, initially developed for concentration and stable isotope measurements of OC and

EC, is suitable for  $^{14}\text{C}$ -based apportionment studies for environment samples, including  $\mu\text{g}$  C-sized samples from Arctic environments.

### 35 1 Introduction

Carbonaceous aerosol is a major component (15-90%) of airborne particulate matter (PM) (Jimenez et al., 2009; Putaud et al., 2010; Yang et al., 2011; Hand et al., 2013; Ridley et al., 2017), and a complex mixture composed of mainly light-scattering organic carbon (OC) and highly-refractory, light-absorbing elemental carbon (EC, also referred to as black carbon) (Pöschl, 2005). The OC and EC fractions play important and often distinct roles in climate (Bond et al., 2013; Hallquist et al., 2009; 40 Kanakidou et al., 2005; Laskin et al., 2015), air pollution and human health (Cohen et al., 2017; Grahame et al., 2014; Janssen et al., 2012). Moreover, both OC and EC were identified as short lived climate forcers (SLCFs) by the IPCC expert meeting ([https://www.ipcc-nkgip.iges.or.jp/public/mtdocs/1805\\_Geneva.html](https://www.ipcc-nkgip.iges.or.jp/public/mtdocs/1805_Geneva.html)) in 2018. To develop and monitor the efficiency of mitigation strategies for both climate change and air pollution, it is required to have a better understanding of the temporal and spatial dynamics of OC and EC emission sources.

45 The majority (>50%) of carbonaceous aerosol is OC, which has a wide size range. Coarse OC (in  $\text{PM}_{10}$ ) consists of plant debris, microorganisms, fungal spores, and pollen. Fine OC (in  $\text{PM}_{2.5}$ ) is formed predominantly via the oxidation or nucleation/coagulation of volatile organic compounds, such as mono- and sesquiterpenes, from both biogenic and anthropogenic sources (Shrivastava et al., 2017), but can also be directly emitted from combustion sources (Hallquist et al., 2009; Fuzzi et al., 2015; Liggio et al., 2016). In contrast, EC is found primarily in fine particles, e.g.,  $\text{PM}_{1.0}$  or smaller (Chan 50 et al., 2013; Bond et al., 2013). It is emitted through incomplete combustion of fossil fuels and biomass/biofuels (Bond et al., 2013; Huang et al., 2010; Evangelou et al., 2016; Winnie et al., 2016; 2017; 2019).

Measuring the isotopic signature and composition, i.e. radiocarbon ( $^{14}\text{C}$ ) content and stable isotope ratio ( $^{13}\text{C}/^{12}\text{C}$ ) of aerosol, offers a powerful tool for quantifying the sources of bulk aerosol and its OC and EC fractions. Aerosol  $^{14}\text{C}$  content can be used to quantify the relative contributions from contemporary biomass and fossil sources (Heal, 2014).  $^{14}\text{C}$  is a naturally 55 occurring radioisotope (5,730-year half-life) produced in the atmosphere. After its oxidation to carbon dioxide ( $^{14}\text{CO}_2$ ),  $^{14}\text{C}$  enters the food chain through photosynthesis so that all living organisms are labeled with a characteristic  $^{14}\text{C}/^{12}\text{C}$  ratio and described as “modern” carbon. Materials containing carbon older than about 50,000 years ( $^{14}\text{C} << ^{12}\text{C}$ ) are described as “fossil” carbon. Over the past centuries, the  $^{14}\text{C}$  content of the atmosphere has undergone distinct changes (Graven, 2015; 60 2020; Levin et al., 2010). Anthropogenic combustion of fossil fuels emit  $^{14}\text{C}$ -depleted carbon into the atmosphere (i.e. dilute the proportion of  $^{14}\text{C}$  relative to  $^{12}\text{C}$ ). In contrast, nuclear weapons testing doubled the  $^{14}\text{C}$  content of  $\text{CO}_2$  in the Northern Hemisphere in the mid-20<sup>th</sup> century, followed by mixing of this bomb-derived  $^{14}\text{C}$ -enriched carbon into the ocean and biosphere. Similarly, aerosol stable isotope ratios provide insight to different types of anthropogenic sources (e.g. combustion of solid and liquid vs. gaseous fossil fuels). However,  $^{13}\text{C}$  data cannot distinguish emissions from mixed fossil fuel combustion and live C3 plant biomass (Huang et al., 2006; Winiger et al., 2016). Thus, isotope-based source apportionment 65 studies become particularly insightful when both  $^{14}\text{C}$  and stable carbon isotopes are considered (Andersson et al., 2015; Winiger et al., 2016, 2017) or when combined with analyses of specific source tracers, such as levoglucosan or potassium for

**Commented [CC2]:** Change to newer paper  
Graven, H., Keeling, R. F., & Rogelj, J. (2020). Changes to Carbon Isotopes in Atmospheric  $\text{CO}_2$  over the Industrial Era and into the Future. *Global biogeochemical cycles*, 34(11), e2019GB006170.

wood burning emissions (Szidat et al., 2006; Zhang et al., 2008) and/or remote sensing data and modeling analysis (Barrett et al., 2015; Mouteva et al., 2015b; Wiggins et al., 2018).

The objective of this study is to evaluate the effectiveness of separating OC and EC via the ECT9 (EnCan-Total-900)

70 protocol (Huang et al., 2006; Chan et al. 2010; Chan et al., 2019) for  $^{14}\text{C}$ -based source apportionment studies of carbonaceous aerosols. The ECT9 technique was originally developed to physically separate OC and EC mass fractions for concentration quantification and stable carbon isotope analysis. This protocol has been used since 2006 to monitor carbonaceous aerosol mass concentrations and stable isotope composition over Canada, including in the Arctic at Alert, as part of the Canadian Aerosol Baseline Measurements (CABM) Network by Environment & Climate Change Canada (Chan et al., 2010; 2019; Eckhardt et al., 2015; Sharma et al., 2017; Xu et al., 2017; Leaitch et al., 2017; 2018; Huang, 2018). It has also been used to monitor carbonaceous aerosol over China (Yang et al., 2011). Furthermore, EC concentration measurements made with the ECT9 protocol correlate well with those derived from light absorption by an aethalometer as well as refractory black carbon (rBC) using a Single Particle Soot Photometer (SP2) (Sharma et al., 2017; Chan et al., 2019). It was demonstrated that the ECT9 protocol can be used to quantify OC/EC concentrations and provide source information at the same time.

80 The ECT9 protocol is a thermal evolution analysis (TEA) protocol which is different from commonly used thermal optical analysis (TOA) methods for monitoring air quality, such as the Interagency Monitoring of Protected Visual Environments (IMPROVE) protocol (Chow et al., 2001; Watson et al., 2007), the National Institute for Occupational Safety and Health protocol (NIOSH method 5040, Birch, 2002), as well as the European Supersites for Atmospheric Aerosol Research (EUSAAR) protocol (Cavalli et al., 2010). In those protocols, the OC fraction is thermally desorbed from filter samples in an 85 inert helium (He) atmosphere at relatively lower temperatures and the EC fraction is combusted at higher temperatures by introducing oxygen ( $\text{O}_2$ ) in He stream while the filter reflectance or transmittance for a laser signal is continuously monitored. During the analysis, a fraction of the OC may char (forming pyrolyzed OC or  $\text{PyOC}$ ), causing the transmittance or reflectance to decrease. While TOA methods use the changes in laser signal to mathematically correct for  $\text{PyOC}$  within the measured EC fraction, the ECT9 protocol aims to minimize or remove  $\text{PyOC}$ , together with carbonate carbon (CC), during an 90 intermediate temperature step of 870°C in pure He via high temperature evaporation (Chan et al., 2019). With much longer retention times at each temperature step (see Methods) and without either reflectance or transmittance used, the ECT9 protocol effectively isolates OC,  $\text{PyOC+CC}$ , and EC.

95 It should be noted that other methods have been also developed mainly for  $^{14}\text{C}$  analysis of OC and EC, such as the CTO-375 (Zencak et al., 2007), the Swiss\_4S protocol (Mouteva et al., 2015a; Zhang et al., 2012), or hydropyrolysis (Meredith et al., 2012; Zhang et al., 2019), which use distinct temperature protocols, gas mixture and/or remove water-soluble OC or inorganic carbon prior to EC analysis. In contrast to the ECT9 protocol, however, these approaches differ substantially from the protocols that are widely used for monitoring OC/EC mass concentrations in the field, which limits the relevance of this data for improving the representation of carbonaceous aerosols in chemical transport models.

100 Here we analyzed the  $^{14}\text{C}$  content of OC and EC fractions (<100  $\mu\text{g C}$ ) isolated with the ECT9 protocol from four pure fossil and contemporary reference materials. These materials were analyzed on their own to quantify the amount and source (modern or fossil) of extraneous carbon introduced by the procedure as well as its reproducibility. Mixtures of two reference materials were measured to elucidate how efficiently the ECT9 protocol isolates OC from EC. In addition, we investigated

the laser signals of three reference materials and three aerosol samples (tailpipe emissions, ambient aerosol from Alert, and SRM8785) to assess how efficiently the ECT9 protocol removes PyOC. Our evaluation of the ECT9 protocol on its ability to 105 physically separate OC from EC for <sup>14</sup>C-based source apportionment studies significantly expands the existing opportunities for characterizing and monitoring sources of carbonaceous aerosol at regional or global scales at the same time providing solid base for EC and OC concentration measurements.

## 2 Methods

### 2.1 The ECT9 protocol for the physical separation of OC and EC

110 The ECT9 protocol was developed at the carbonaceous aerosol & isotope research (CAIR) lab of Environment and Climate Change Canada (ECCC) to quantify the amount of OC and EC in carbonaceous aerosol and their  $\delta^{13}\text{C}$  values (Huang et al., 2006; Chan et al., 2010; 2019). Carbon fractions are isolated with an OC/EC analyzer (Sunset Laboratory Inc.) coupled to a custom-made gas handling and cryogenic trapping system for  $\text{CO}_2$  collection from OC and EC fractions (Fig. 1a). The 115 fractions are separated from each other, according to their degree of [refractorinessrefractory](#). Specifically, carbon fractions are released by the ECT9 protocol in three steps (Fig. 1b): (1) OC at 550°C for 600 seconds in pure He (99.9999% purity); (2) PyOC and CC at 870°C for 600 seconds in pure He; and (3) EC at 900°C for 420 seconds in a mixture of 2%  $\text{O}_2$  with 98% He. All fractions are fully oxidized to  $\text{CO}_2$  by passing through a furnace containing  $\text{MnO}_2$  maintained at 870°C. For concentration determination, the  $\text{CO}_2$  passes through a methanator at 500°C, is converted to  $\text{CH}_4$ , and quantified with a flame 120 ionization detector. For isotope analysis, the  $\text{CO}_2$  is cryo-trapped with liquid  $\text{N}_2$  (-196°C) in a U shaped glass trap, purified on a vacuum system (to remove He), sealed into a Pyrex ampoule, and analyzed for its  $\delta^{13}\text{C}$  ratio with an Isotopic Ratio Mass Spectrometer (IRMS), i.e., MAT253 or [FIM](#)<sup>14</sup>C with an Accelerated Mass Spectrometer (AMS).

### 2.2 Reference materials and their composition

To evaluate the ECT9 method for separating OC and EC for <sup>14</sup>C analysis, we isolated and measured the  $^{13}\text{C}$  and <sup>14</sup>C content of the OC or EC fraction or TC from 5-6 modern or fossil reference materials (Table 1), including two pure OC (adipic acid, 125 sucrose), two EC (C1150, regal black), and two natural OC/EC-mixtures (rice char and urban dust SRM1649a).

Some of the reference materials have previously been utilized to compare different protocols that quantify OC/EC fractions (Hammes et al., 2007; Willis et al., 2016) as well as determine the mass of extraneous carbon introduced during OC/EC isolation from carbonaceous aerosol (Mouteva et al., 2015a). Table 1 provides an overview of their chemical compositions, i.e., total carbon contents and relative fraction of OC and EC, respectively (for individual measurements see Table S1). 130 Primary methods (i.e., gravimetric or volumetric) are used for mass loading of the materials, whereas the mass of TC, OC, and EC are quantified via the ECT9 thermal protocol. Based on repeat injections of sucrose results (20-80  $\mu\text{g}$  sucrose,  $n = 117$ ), the accuracy of the TC mass is about 5%. The reproducibilities of both OC/TC and EC/TC percentages are 2% or better. Although uncertainties of weighing pure EC mass (i.e., Regal black and C1150) via microbalances are relatively large (due to static electricity and variable relative humidity), the EC/TC and OC/TC ratios for all reference materials are highly

135 reproducible (one s.d. <2%). The results show that the two EC materials (i.e., regal black and C1150) contain 97% and 98% EC, with only 3% and 2% OC, respectively. The two OC materials (i.e., sucrose and adipic acid) are 99% and 100% OC, and less than 1% EC (likely due to charred OC contribution), respectively. Thus, the materials are suitable for the purpose of this study.

140 We also analyzed the  $^{13}\text{C}$  and  $^{14}\text{C}$  isotopic composition of each reference material, using off-line combustions and ECT9 coupled with cryo-purification to convert them into  $\text{CO}_2$ . The results are summarized in Table 2 (for individual results see Tables S2 & S3). The  $^{14}\text{C}$  analysis of  $\mu\text{g}$  C-sized carbonaceous aerosol samples requires the assessment of extraneous carbon (Santos et al., 2010). This is achieved by measuring multiple smaller-sized materials with known  $^{14}\text{C}$  content. Consequently, the results in Table 2 are critical, as those  $^{14}\text{C}$  values provide the reference for quantifying the extraneous carbon introduced during the isotope analysis procedures.

#### 145 2.3 Isolation of OC, EC or TC with the ECT9 protocol and purification of $\text{CO}_2$

The isotopic analysis of carbonaceous aerosol via the ECT9 system involves three steps (Fig. 1a): 1) OC and EC isolation/ $\text{CO}_2$  collection and 2)  $\text{CO}_2$  purification, followed by 3) isotope analysis for either  $^{13}\text{C}/^{12}\text{C}$  by IRMS or  $^{14}\text{C}$  by AMS (i.e., coupled measurements of  $^{13}\text{C}/^{12}\text{C}$  and  $^{14}\text{C}/^{12}\text{C}$  of  $\mu\text{g}$  C-sized graphite targets), as desired.

150 The initial masses of the pure reference materials ranged from 5 to 47  $\mu\text{g}$  C (n=3-13; Table S6), whereas those for the mixed materials ranged from 5-30  $\mu\text{g}$  C for OC and 5-60  $\mu\text{g}$  C for EC (n=5-6; Table S7). The loaded mass of each material was determined via a microbalance (MX5, Mettler Toledo or CCE6, Sartorius) with the lowest reading to 1  $\mu\text{g}$  C or 0.1  $\mu\text{g}$  C, respectively. Filters before mass loading were pre-combusted at 900°C in a muffle furnace overnight and wrapped into pre-fired aluminum foil before cooling below 200°C. Usually, OC materials were first dissolved in MQ-water with known volume to obtain its concentration, and then a known amount (5-10  $\mu\text{l}$ ) of OC solution was very carefully applied onto a pre-cleaned quartz filter surface (1.5 cm<sup>2</sup>, Pall Canada Limited) via a syringe injection. After the injection, the quartz boat holding the punch is pushed to the right position inside of the analyzer. The volume of OC solution used does not saturate the filter, but merely moistens the surface. After purging the filter for about 20 minutes ensuring the water is gone, the filter is ready for analysis. EC (i.e., Regal black and C1150) and mixed materials (rice char or SRM 1649a), which cannot be completely dissolved in water, were directly weighed onto pre-cleaned quartz filter punches in form of solids (powders). 155 Adipic acid were also loaded as powder. The final power mass was determined by the difference weighted before and after analysis. These filters were pre-combusted at 900°C in a muffle furnace overnight and wrapped into pre-fired aluminum foil before cooling below 200°C. A filter punch with the loaded mass was carefully carried to the Sunset analyzer by a Pyrex glass Petri dish with cover for analysis put into the Sunset analyzer and analyzed with the ECT9 protocol.

OC and EC were separated and the combusted OC or EC fractions as  $\text{CO}_2$  were cryo-collected in a U-shaped flask 160 submerged in liquid  $\text{N}_2$  (Fig. 1a, step 1). Then, this flask containing  $\text{CO}_2$  and He was connected to a vacuum line with 4 cryo-traps and several open ports (Fig. 1a, step 2), where the  $\text{CO}_2$  is purified by sequential distillation when passing cryo-traps 1 through 3. Finally the pure  $\text{CO}_2$  is transferred and sealed into a 6 mm glass ampoule for  $^{13}\text{C}$  or  $^{14}\text{C}$  analysis. -Pressure is read

**Commented [H3]:** This content was added to address the comments by both reviewer#1 and reviewer#2 on section 2.3 for loading dissolved materials onto filters.

by a Pirani gauge before sealing the ampoule for an estimation of the amount of gas, and consequently, sample size could be determined as  $\mu\text{g C}$  also determination as  $\mu\text{g C}$ .

170 **2.4  $^{14}\text{C}$  measurements (graphitization & AMS analysis)**

At the KCCAMS facility, the OC and EC fractions or TC (in form of  $\text{CO}_2$ ) were reduced to graphite on iron powder via hydrogen ( $\text{H}_2$ ) reduction using equipment and protocols specifically developed for smaller-sized ( $\leq 15 \mu\text{g C}$ ) samples (Santos et al., 2007b; 2007a). Briefly, sample- $\text{CO}_2$  was introduced into a vacuum line, cryogenically isolated from any water vapor, monometrically quantified, and then transferred to a heated reaction chamber, where it was mixed with  $\text{H}_2$  and reduced to filamentous graphite. To characterize the graphitization, handling and AMS analysis, two relevant standards (Oxalic Acid II as modern carbon and Adipic acid as fossil carbon), with similar size ranges of the samples prepared via ECT9, were also processed into graphite. The graphite was then pressed into aluminum holders and loaded into the AMS unit alongside measurement standards (Table S6) and blanks for  $^{14}\text{C}$  measurement (Beverly et al., 2010). The data are reported in fraction modern carbon ( $\text{FM}^{14}\text{C}$ ), following the conventions established by Stuiver and Polach (1977) and also described elsewhere (Reimer et al., 2004; Trumbore et al., 2016).

180 To establish consensus values (Table 2), we also analyzed the  $^{14}\text{C}$  content of the bulk reference materials ranging in size from 0.06 to 1 mg C, using our standard combustion and graphitization methods. Larger aliquots of material were weighed into pre-combusted quartz tube with 80 mg  $\text{CuO}$ , evacuated, and combusted at  $900^\circ\text{C}$  for 3 hours. The resulting  $\text{CO}_2$  was cryogenically purified on a vacuum line, reduced to graphite using a closed-tube zinc-reduction method (Xu et al., 2007), and analyzed as described above.

**Commented [H4]:** Gua/Claudia: should this reference be replaced by Reimer et al. (2004)?

**Commented [CC5R4]:** I would just use "F" and cite Trumbore et al. 2016

**2.5 Quantification of extraneous carbon**

Any type of sample processing and analysis introduces extraneous carbon ( $\text{C}_{\text{ex}}$ ). Therefore, the measured mass of any sample will include the mass of this sample and of any  $\text{C}_{\text{ex}}$  incorporated throughout the analysis [Eq. 1]:

$$m_{\text{spl,meas}} = m_{\text{spl}} + m_{\text{ex}} \quad [\text{Eq. 1}],$$

190 where  $m_{\text{spl,meas}}$ ,  $m_{\text{spl}}$ , and  $m_{\text{ex}}$  are the measured and theoretical mass of the sample and of  $\text{C}_{\text{ex}}$ , respectively. For small samples (with a mass of a few  $\mu\text{g C}$ ), the mass of  $\text{C}_{\text{ex}}$  can compete with or overwhelm the sample mass and cause the measured  $\text{FM}^{14}\text{C}$  value of a sample to deviate from its consensus value.

Here, we estimated the mass of  $\text{C}_{\text{ex}}$  introduced during the ECT9 protocol and the  $^{14}\text{C}$  analysis following Santos et al. (2010), where  $\text{C}_{\text{ex}}$  is understood to consist of a modern and of fossil component [Eq. 2]:

$$195 m_{\text{ex}} = m_{\text{mex}} + m_{\text{fex}} \quad [\text{Eq. 2}],$$

where  $m_{\text{mex}}$  and  $m_{\text{fex}}$  is the mass of the modern and fossil  $\text{C}_{\text{ex}}$ , respectively.

Following an isotope mass balance approach, the measured isotopic ratio ( $^{14}\text{C}/^{12}\text{C}$ ) of a sample ( $R_{\text{spl,meas}}$ ) can be expressed as [Eq. 3].

$$R_{spl\_meas} = \frac{m_{spl}R_{spl} + m_{mex}R_m + m_{fex}R_f}{m_{spl\_meas}} \quad [\text{Eq. 3}],$$

200 where  $R_{spl}$  is the theoretical isotopic ratio of the sample, and  $R_m$  and  $R_f$  are the consensus isotopic ratios of a modern and fossil standard, respectively. This equation can be further simplified because  $R_f$  is 0.  $R_m$  is determined by measuring regular-sized aliquots of this reference material. In addition, all  $^{14}\text{C}/^{12}\text{C}$  ratios are corrected for isotope fractionation using their  $\delta^{13}\text{C}$  measured alongside  $^{14}\text{C}$  on the AMS (Beverly et al., 2010).

205 The mass of modern  $\text{C}_{\text{ex}}$  can be quantified by analyzing fossil reference materials, which are highly sensitive to modern and insensitive to fossil pollutants. Based on [Eq. 3] the measured isotopic ratio of the fossil reference ( $R_{f\_meas}$ ) can be expressed as [Eq. 4]:

$$R_{f\_meas} = \frac{m_{mex}R_m}{m_{spl\_meas}} \quad [\text{Eq. 4}]$$

The smaller the mass of the fossil reference material, the greater the effect of the constant mass of modern  $\text{C}_{\text{ex}}$  on the isotope ratio of the fossil reference material, i.e.  $R_{f\_meas}$  deviates toward  $R_m$ .

210 Similarly, the mass of fossil  $\text{C}_{\text{ex}}$  can be quantified by analyzing modern reference materials. With decreasing mass, the measured isotopic ratio of the modern reference ( $R_{m\_meas}$ ) will deviate more strongly from  $R_m$  (toward  $R_f$ ).

Based on [Eq. 1-3] and assuming  $m_{spl} \gg m_{mex}$ , the  $R_{m\_meas}$  can be expressed as [Eq. 5]:

$$R_{m\_meas} = \frac{m_{spl}R_m + m_{mex}R_m}{m_{spl\_meas}} \approx \frac{(m_{spl\_meas} - m_{fex})R_m}{m_{spl\_meas}} \quad [\text{Eq. 5}]$$

Finally, we can calculate the  $\text{C}_{\text{ex}}$ -corrected isotope ratio of an unknown sample ( $FM_{spl\_cor}$ ). This value reported as

215 the ratio between the theoretical isotopic ratio of this sample and the accepted value of a modern standard ( $R/R_m$ ) also known as Fraction Modern ( $FM$ ; with all  $R$  corrected for stable isotope fractionation). This data is reported as [Eq. 6]:

$$FM_{spl\_cor} = \frac{R_{spl}}{R_m} \approx \frac{R_{spl\_meas} - R_{f\_meas}}{R_{m\_meas} - R_{f\_meas}} \approx FM_{m*} \times \frac{\left[ \frac{R_{spl\_meas}}{R_m} - \frac{m_{mex}}{m_{spl\_meas}} \right]}{\left[ \frac{1 - m_{mex}}{m_{spl\_meas}} - \frac{m_{fex}}{m_{spl\_meas}} \right]} \quad [\text{Eq. 6}],$$

220 where  $FM_{m*}$  is determined from the direct measurement of the modern primary reference material (OX1) used to produce six time-bracketed graphite targets measured in a single batch, after isotopic fractionation correction and normalization (Santos et al., 2007a,b). The individual uncertainty of  $FM_{spl\_cor}$  is determined from counting statistics and by propagating the quantified blanks using a mass balance approach. Long-term and continuous measurements of various types of blanks indicate that the mass of  $\text{C}_{\text{ex}}$  within one analytical method or system can vary as much as 50% (see Santos et al., 2010; Fig. 1). Therefore, we applied a 50% error in  $m_{fex}$  and  $m_{mex}$  from long-term 225 measurements of variance in  $m_{ex}$  of small samples (Santos et al., 2007a).

In this study, we used a multi-step approach to quantify  $m_{ex}$  introduced by the ECT9 protocol and  $^{14}\text{C}$  analysis (i.e., graphite target preparation for  $\text{CO}_2$  sample plus AMS analysis). First, we quantified  $m_{ex}$  introduced during  $^{14}\text{C}$

sample preparation and analysis by analyzing different masses of our bulk reference materials [without involving ECT9 protocol](#). Extraneous carbon is introduced during sealed tube combustion and graphitization followed by 230 graphite target handling and [AMS measurement at the KCCAMS facility](#). Typically, <sup>14</sup>C [sample preparation and analysis- AMS measurement](#) contributes a small portion to  $m_{ex}$  (Mouteva et al., 2015a; Santos et al., 2010). Second, we quantified the portion of  $m_{ex}$  added during the isolation of OC and EC with the ECT9 protocol. This portion of  $m_{ex}$  allows us to determine the practical minimum sample size limit for the entire method, including  $m_{ex}$  contributions from filter handling before OC/EC analysis, instrument separation, and transfer to cryo-collection 235 system and Pyrex ampoules. To isolate this portion, we quantified  $m_{ex}$  of the entire procedure (ECT9 protocol plus <sup>14</sup>C analysis) by analysing the <sup>14</sup>C signature of OC and EC from different masses of a large set of reference materials, and then subtracted the portion of  $m_{ex}$  introduced during <sup>14</sup>C analysis.

### 3. Results and Discussion

#### 3.1. Recovery estimation

240 The reference materials used in this study, including the modern and fossil endmembers (i.e., the major carbon sources) found in carbonaceous aerosol, and their TC, OC, and EC concentrations are shown in Table 1. -Reference materials were separated into OC, EC, or TC using the ECT9 method at ECCC's CAIR lab (Fig. 1) and analyzed for their <sup>14</sup>C content at UC Irvine's KCCAMS facility. [including graphitization and AMS analysis](#).

245 Fig. 2 shows the cross-validation of carbon-mass between the mass determined at ECCC's CAIR lab and the mass quantified at UC Irvine's KCCAMS lab indicating a very good positive correlation ( $R^2 = 0.93$  for pure materials and  $R^2 = 0.95$  for two-material-mixtures in Fig. 2a and 2b, respectively). [Reassessment of sample masses by manometric measurements at UCI show good agreement with initial mass loaded at ECCC's CAIR lab via gravimetric or volumetric methods \(Fig. 2a,2b and Table 6S and 7S\)](#). It is suggested that no major losses or gains of carbon occurred during the entire analytical process and the overall recovery was close to 100%, with a 5% uncertainty for 250 samples ranging in size from about 5 to 60  $\mu\text{g C}$ .

#### 3.2 Quantification of extraneous carbon and its sources

All types of samples, regardless of size, show deviations in their measured  $\text{FM}^{14}\text{C}$  value from their consensus values to 255 certain degree due to  $C_{ex}$  introduced during sample analysis. In  $\mu\text{g C}$ -sized samples (mass  $< 15 \mu\text{g C}$ ), significant bias from any  $C_{ex}$  can be observed, because  $C_{ex}$  constitutes a large fraction of the total sample. Previous work (using solvent-free analytical protocols) has shown that modern  $C_{ex}$  is introduced mostly through instrumentation and sample handling techniques, while fossil  $C_{ex}$  originates from iron oxide used as a catalyst for the reduction of  $\text{CO}_2$  to graphite prior to AMS analysis (Santos et al., 2007a; 2007b).

The  $\text{FM}^{14}\text{C}$  values of the pure modern or fossil reference materials generally agreed with their accepted  $\text{FM}^{14}\text{C}$  values for both OC and EC fractions (within approximately 5% uncertainty on average, Fig. 3 and [Table 2, Tables S6 & S7](#)) after 260 applying a constant amount  $C_{ex}$  correction in  $\text{FM}^{14}\text{C}$  determination. [Specifically, the overall agreements for all individual](#)

#### Commented [H6]:

This addition was to address a comment below by reviewer#1  
"Line 232. How was the mass determined at the CAIR lab?  
Is it from the integration of the OC/EC signals or from  
manometry? If it is from manometry, it is not a great  
comparison and probably does not warrant a figure."

pure (Table S6) and mixed reference materials (Table S7, excluding the OC data from adipic acid + bulk rice char) are within  $\pm 3\%$  of their corresponding values (Table 2). On average, for samples containing  $>10\text{ }\mu\text{g C}$  the agreements are within  $\pm 1\%$ , whereas samples containing between  $>5\text{ }\mu\text{g C}$  and  $<10\text{ }\mu\text{g C}$  they are around  $7\pm 5\%$ , respectively. This constant  $C_{\text{ex}}$  is a critical prerequisite for accurately correcting the  $\text{FM}^{14}\text{C}$  value of unknown samples. Hence, our data demonstrated that the

265 ECT9 method (and subsequent  $^{14}\text{C}$  analysis) introduces a small, reproducible amount of  $C_{\text{ex}}$ .

According to equations [4]-[5] in section 2.5,  $C_{\text{ex}}$  can be quantified by measuring  $\text{FM}^{14}\text{C}$  of pure modern or fossil materials with different sizes. Fig. 3 demonstrates that regardless what  $^{14}\text{C}$  content are in carbon fractions isolated from the reference materials and what sizes they are, the corrected  $\text{FM}^{14}\text{C}$  values match with consensus value within propagated uncertainty.

To evaluate the suitability of ECT9 for  $^{14}\text{C}$  analysis of aerosol samples, a comparison is made between the results of a published method (i.e., Swiss\_4S) and those of ECT9. The two protocols are listed in Table 3 and their  $C_{\text{ex}}$  distribution is shown in Table 4. The total amount of  $C_{\text{ex}}$  introduced by the complete procedure through ECT9, and determined based on all reference materials, was  $1.3\pm 0.6\text{ }\mu\text{g C}$ , with 70% originating from contamination with modern carbon (Table 4). The isolation of OC and EC with the ECT9 protocol introduced 65% of total  $C_{\text{ex}}$  ( $0.85$  out of  $1.35\text{ }\mu\text{g C}$ ), with 65% derived from modern carbon. Overall, the total amount of  $C_{\text{ex}}$  introduced during OC/EC isolation with the ECT9 protocol is comparable to that for the Swiss\_4S protocol established at UC Irvine within uncertainties (Table 3, Mouteva et al. (2015a)). Thus, it is demonstrated that the ECT9 protocol serves as a suitable alternative for the  $^{14}\text{C}$  analysis of aerosol samples with masses  $>5\text{ }\mu\text{g C}$ .

### 3.3 Effectiveness of OC/EC separation

To investigate the effectiveness of the ECT9 to separate OC from EC in more complex mixtures with minimizing OC into the EC fraction via pyrolysis, mixtures of the modern and fossil reference materials (Table 2) were used for measuring  $\delta^{13}\text{C}$  (Table S4 - S5) and  $\text{FM}^{14}\text{C}$  (Table S7).

First, it was found that the  $\text{FM}^{14}\text{C}$  values of OC and EC fractions isolated from mixtures of pure sucrose (modern OC) and pure regal black (fossil EC) were within the measurement uncertainty of their accepted  $\text{FM}^{14}\text{C}$  values, after correction for a constant amount of  $C_{\text{ex}}$  (Fig. 4) for samples with  $5 - 34\text{ }\mu\text{g OC}$  carbon and  $10 - 60\text{ }\mu\text{g EC}$  carbon, showing a good separation of OC from EC. This amount of  $C_{\text{ex}}$  was identical to that applied to the pure reference materials above, further corroborating the constant background introduced by the ECT9 protocol and  $^{14}\text{C}$  analysis.

Next, the mixtures of fossil adipic acid (pure OC) and modern rice char (mixture of OC and EC) were isolated and analyzed. It was found that after correction for  $C_{\text{ex}}$ , the  $\text{FM}^{14}\text{C}$  values of the OC (from the mixture) were systematically greater than the consensus value of the pure adipic acid, i.e., a  $\text{FM}^{14}\text{C}$  of zero (Fig. 5a), indicating that there was certain level of modern fraction contributed to the measured OC from the modern rice char. Based on an elevated mean value of  $0.1081\pm 0.0259$  ( $n=6$ ) after blank corrections, a mass balance calculation indicates that  $10\pm 3\%$  of OC-Rice char is present. The high end of this estimation is close to  $\sim 14\%$  within a validity range to what one would expect.

To confirm that ECT9 could remove OC contained in rice char, an additional step was taken before mixing modern rice char's EC with the fossil OC (adipic acid). Specifically, we stripped the OC fraction of rice char by running rice char (on a

**Commented [H7]:** This revised content is to address the comment raised by Reviewer #2 as below

“Line 245: It is mentioned that  $\text{FM}^{14}\text{C}$  values of pure modern and fossil reference materials agreed with their accepted  $\text{FM}^{14}\text{C}$  values within approx. 5% uncertainty. Please indicate the individual uncertainties that resulted in less than 5% in average.”

295 filter) through the ECT9 protocol. Adipic acid (fossil OC) was then injected onto the filter with the remaining rice char-EC. The results show that the  $\text{FM}^{14}\text{C}$  of OC values of this mixture lie well within the expected range of the consensus value (Fig. 5b) after a  $\text{C}_{\text{ex}}$  correction as described above, demonstrating an excellent remove of rice char OC.

296 In both mixtures (fossil adipic acid with modern bulk rice char or rice char-EC), the corrected  $\text{FM}^{14}\text{C}$  values of the isolated  
297 EC fractions were within the expected range for the rice char reference material (Fig. 5c, d). This provides further evidence  
300 that the ECT9 protocol isolates modern EC from fossil OC with no obvious evidence of transferring fossil OC into the EC  
fraction. Together, the three sets of mixing experiments (Figs. 4 & 5) provide strong evidence for the effectiveness of  
separating OC from EC via ECT9 protocol.

305 In addition to  $\text{FM}^{14}\text{C}$  measurements,  $\delta^{13}\text{C}$  measurements in mixtures of OC and EC can also provide quantitative information  
on the effectiveness of OC and EC separation via ECT9. Various amounts of sucrose (pure OC, 10 – 30  $\mu\text{g C}$ ) were first  
310 mixed with varying amounts of Regal black (pure EC, 20 – 66  $\mu\text{g C}$ ). The mixtures were then physically separated into OC  
and EC fractions by ECT9 for  $\delta^{13}\text{C}$  measurements. The measured  $\delta^{13}\text{C}$  values of OC and EC from these mixing experiments  
are listed in Table S4. Based on the  $\delta^{13}\text{C}$  values of individual pure reference materials (Table S3) and a two-end-member  
mixing mass balance, it is estimated that the average fraction contributed into each other in the mixtures (i.e., sucrose fraction  
into Regal black or vice versa) was likely less than 3% (Table S5).

### 310 3.4 Charring evaluation & $\text{PyOC}$ removal using the ECT9 protocol

315 It is known that some of OC (e.g., oxygenated OC or water soluble OC) would char to form pyrolyzed organic  
carbon ( $\text{PyOC}$ ) when heated in an inert He atmosphere, darkening the filter (Chow et al., 2004; Watson et al. 2005)  
and causing decreased laser signals due to light-absorption of charred OC. In most TOA protocols, this  $\text{PyOC}$  would  
combust and contribute to EC when  $\text{O}_2$  is added. However,  $\text{PyOC}$  can be also be gasified and released as CO at high  
320 temperatures ( $>700^\circ\text{C}$ ) with limited  $\text{O}_2$  supply, e.g., oxygenated OC at  $870^\circ\text{C}$  (Huang et al., 2006; Chan et al., 2010;  
2019). Most TOA protocols estimate  $\text{PyOC}$  by quantifying the mass associated with reflectance/transmittance  
changes, i.e., the mass released between the time when  $\text{O}_2$  is introduced and the OC/EC split point (where the  
reflectance/transmittance returns to the initial value). In contrast to other TOA protocols, ECT9 defines  $\text{PyOC}$  as the  
mass released at the temperature step of  $870^\circ\text{C}$  (during a period of 600 seconds). This includes charred OC, calcium  
325 carbonate ( $\text{CaCO}_3$ ) that decomposes at  $830^\circ\text{C}$ , and any refractory OC not thermally released at  $550^\circ\text{C}$  (Huang et al.,  
2006; Chan et al., 2010; 2019).

330 Although ECT9 do not use laser signals to quantify  $\text{PyOC}$ , it is expected that the changes of laser signals during the  
stage of  $870^\circ\text{C}$  would provide useful information about  $\text{PyOC}$ . Thus, four sets of samples were selected, including  
335 those of pure reference materials and ambient aerosol samples from different sources with heavy or light mass  
loading (e.g., those Arctic sample filters from different seasons) to evaluate the possible charring via ECT9. Their  
thermograms are shown in Figures 6 to 9.

Figure 6 shows thermograms of pure or bulk references for Regal black, sucrose, and rice char, respectively. It is  
observed in all three that the laser transmittance signals first decrease and then increases again during the  $870^\circ\text{C}$

step, and that they return to their initial values just before EC is released at the next step of 900°C. This

330 demonstrates that the ECT9 method minimizes PyOC-contributions to the EC fraction.

The thermograms of aerosol (on filters) collected directly from tailpipe exhaust of a diesel engine vehicle and a gasoline engine passage car, respectively are shown in Figure 7. These data suggest that the amount of PyOC generated during analysis are sample/matrix dependent. Specifically, the mass fraction during the 870°C

temperature is larger for the gasoline than the diesel engine. This finding supports previous work showing that

335 PyOC is proportional to the amount of oxygenated OC (Chan et al., 2010). It is noticed that the laser signal reaches the initial value before the EC step, further demonstrating that the charring contribution to EC is minimized.

Another set of thermograms of two total suspended particle filter samples collected during the summer (August) and winter (December) of 2015 at an Arctic site (i.e., Alert) are shown in Figure 8. More details about these samples can be found in Wex et al. (2019). The laser signal patterns are similar to those shown in Figures 6 & 7, yet more

340 pronounced. During the 550°C step, the laser signals decrease. During the 870°C step, the signals further decrease, then increase, and finally increase to their initial point before EC is released at 900°C. These thermograms further demonstrate ECT9 is able to minimize PyOC by gasification.

Finally, the thermographs of NIST urban dust reference material SRM 8785 (the re-suspended SRM 1649a urban dust with a fine fraction <2.5  $\mu$ m collected on quartz filter) analyzed with ECT9 and Swiss\_4S are shown in Figure

345 9. Both thermograms obtained with the ECT9 method (Fig. 9 a&b) show the similar patterns as those in Figs. 6-8, i.e., the laser signals reaching the initial value just before the EC release at 900°, suggesting that the charring contribution to EC is minimized during the stage of 870°C even though some PyOC might remain.

In the thermogram obtained with the Swiss-4S protocol (Fig. 9c), the laser signal increases from the beginning of the run while the first two stages (375°C and 475°C) are under the conditions of pure O<sub>2</sub> stream, inferring that light

350 absorbing carbon is released during the first two OC stages. The laser signal continues to increase while the temperature increases up to 650°C (the third stage) under the pure He gas stream, indicating that no charred OC is formed. However, when the temperature starts decreasing from 650°C, the laser signal decreases, indicating PyOC formation below that temperature. This signal decrease continues until the beginning of the next pure O<sub>2</sub> stage. It is important to note that to obtain EC fraction, the Swiss-4 (Table 3) method calls for filter sample pre-treatment, i.e., 355 extraction with water before the thermal separation of OC/EC to minimize the contribution of charred OC from the 3<sup>rd</sup> stage to EC at the 4<sup>th</sup> stage (Zhang et al., 2012). However, for a method comparison, the thermogram shown in Fig. 9c was from a filter without pre-treatment. While it is difficult to make direct comparisons between OC and EC from b) and c) in Figure 9, the laser profiles from those thermograms in Fig. a) and b) indicate that in both cases charred OC is negligible or minimum via ECT9.

360 Together, the thermograms (Figs. 6-9) elucidate that the ECT9 protocol can effectively remove or minimize charred OC (PyOC) to achieve good physical separation of OC and EC. Another great advantage of using ECT9 to separate OC from EC for isotope analysis (both <sup>13</sup>C & <sup>14</sup>C) is its consistency with the protocol used for OC and EC

concentration measurements. Moreover, the ECT9 method does not require filter samples to be pre-extracted with water before EC analysis (to reduce PyOC).

365 **4. Conclusions**

We demonstrate the effectiveness of the ECT9 protocol to physically isolate OC and EC from aerosol samples for  $^{14}\text{C}$  and  $^{13}\text{C}$  analysis by using OC and EC reference materials on their own and as mixtures. It was found that the ECT9 protocol successfully separates OC and EC fractions with a low (but largely modern) total carbon blank of  $1.3 \pm 0.6 \mu\text{g C}$ . The majority (65%) of this extraneous carbon originates from the isolation with the ECT9 protocol, 370 with 35% contributed from graphitization and  $^{14}\text{C}$  measurement of the samples at the KCCAMS facility. After mass balance background corrections, the FM $^{14}\text{C}$  results from both bulk pure materials and mixtures (with sample size as small as 5  $\mu\text{g C}$ ) can reach the consensus values (Table 2) with an average uncertainty of about 5%.

In addition, we evaluated potential PyOC formation during ECT9 by investigating thermograms of a variety of reference materials and ambient filter samples. It is demonstrated that ECT9 provides a good alternative for 375 carbonaceous aerosol source apportionment studies, including ultra small sized (5-15  $\mu\text{g C}$ ) samples obtained from Arctic regions. To increase the application of isotope data ( $^{14}\text{C}$  or  $^{13}\text{C}$ ) in atmospheric research, future efforts should be focused on the comparison on OC/EC separation via different methods/protocols using the same sets of reference materials. At the same time, the isolation results should be also compared among those methods/protocols widely used in long-term national monitoring network for OC/EC contents, ensuring a consistency in measurements 380 between OC/EC concentrations and their corresponding isotopic compositions.

**Nomenclature**

AMS	Accelerator Mass Spectrometry
ASTD	Atmospheric Science & Technology Directorate
BC	Black carbon
385 CABM	Canadian Aerosol Baseline Measurement
CAIR	Carbonaceous Aerosol & Isotope Research
CCMR	Climate Chemistry Measurements and Research
CC	Carbonate carbon
CRD	Climate Research Division
390 EC	Elemental carbon
ECCC	Environment and Climate Change Canada
ECT9	EnCan-Total-900 protocol
EUSAAR	European Supersites for Atmospheric Aerosol Research
FID	Flame ionization detector

395	FM <sup>14</sup> C	Fraction Modern Carbon
	ICP	Inter-comparison study
	IRMS	Isotopic Ratio Mass Spectrometer
	IMPROVE	Interagency Monitoring PROtected Visual Environments
	KCCAMS	W.M. Keck Carbon Cycle Accelerator Mass Spectrometry Facility
400	MAC	Mass absorption coefficient
	NIST	National Institute of Standard and Technology
	OC	Organic carbon
	PM	Particulate matter
	PyOC	Pyrolyzed organic carbon
405	PSAP	Particle Soot Absorption Photometer
	rBC	Refractory Black Carbon
	SP2	Single Particle Soot Photometer
	SRM	Standard Reference Material
	TC	Total carbon
410	TEA	Thermal evolution analysis
	TOA	Thermal optical analysis
	UCI	University of California, Irvine

#### **Data availability**

All data presented in this article are included in the supplement.

#### **415 Supplement**

The supplement related to this article is available online at: <https://doi.org/10.5194/amt-2020-201-supplement>. (to be finalized)

#### **Author contributions**

Conceptualizing and designing the study: LH, CIC, and GMS

420 Developing analytical methods and ensuring data quality: LH, GMS, WZ, CIC, BTR

Performing the experiments and data acquisition: WZ, GMS, SRH, VV, BTR

Data organizing /analysis and interpretation: LH, CIC, BTR, GMS, WZ

Writing the paper, including editing and preparing figures and tables: LH, CIC, BTR, GMS, WZ

**Competing interests**

425 The authors declare that they have no conflicts of interest.

**Acknowledgements**

This research was supported by A-base funding from Environment and Climate Change Canada and the KCCAMS Facility at the University of California, Irvine through G.M.S. We thank D. Enrst (ECCC) and J. Southon (KCCAMS) for supporting  $^{13}\text{C}$ - IRMS and  $^{14}\text{C}$ -AMS analyses, respectively.

**Table 1.** Overview of the bulk reference materials analyzed with the ETC9 method for their total carbon (TC), organic carbon (OC), and elemental carbon (EC) contents.

Reference material	EC				OC				EC + OC mixture			
	Regal black		C1150		Sucrose		Adipic acid		Rice char		SRM-1649a	
	mean	s.d.	mean	s.d.	mean	s.d.	mean	s.d.	mean	s.d.	mean	s.d.
TC (%)	96	9	98	12	101 <sup>a</sup>	4	43 <sup>b</sup>	5	52 <sup>c</sup>	1	17.9 <sup>d</sup>	1.1
OC/TC (%)	<b>3</b>	1	<b>1</b>	2	<b>99</b>	1	<b>100</b>	0	<b>14</b>	1	<b>51.5</b>	0.8
EC/TC (%)	<b>97</b>	1	<b>99</b>	2	<b>1</b>	1	<b>0</b>	0	<b>86</b>	1	<b>48.5</b>	0.8
n	41		24		117		5		6		6	
Bulk material	fine powder			solution		fine powder						
Loading method	gravimetric (via a balance with 1 - 0.1 µg accuracy)				volumetric injection		gravimetric (1 - 0.1 µg accuracy)					
Loading range (µg)	16 - 134		4 - 104		20 - 80		30 - 250		70 - 210		440 - 1100	
Analysis period	2015 – 2017		2006, 2013, 2015		2013 - 2018		2015, 2019		2018		2004 - 2005	
Supplier	Aerodyne Research, MA, USA	McMaster Univ., ON, Canada	Sigma-Aldrich, MO, USA	Fisher-Scientific, NH, USA	Univ. of Zurich, Switzerland		NIST, MD, USA					

<sup>a</sup>101% is obtained from the ratio of TC measured to TC calculated from the injected solution of sucrose; <sup>b</sup>49% of TC to bulk material in adipic acid based on its molecular mass; <sup>c</sup>8.6% of TC to bulk material in Rice char obtained from Hammes et al. (2006); <sup>d</sup>17% of TC to bulk material in SRM 1649a obtained from a critical evaluation of inter-laboratory data by Currie et al. (2002)

**Table 2.** Overview of the isotopic composition of the reference materials used in this study. Radiocarbon ( $^{14}\text{C}/^{12}\text{C}$ , reported as fraction modern (FM $^{14}\text{C}$ )) was measured at the KCCAMS facility and  $\delta^{13}\text{C}$  at the CAIR lab.

Reference material	EC				OC				EC + OC mixture													
	Regal black		C1150		Sucrose		Adipic acid		Rice char		SRM-1649a											
	mean	s.d.	mean	s.d.	mean	s.d.	mean	s.d.	mean	s.d.	mean	s.d.										
<b><math>^{14}\text{C}</math> analysis</b>																						
FM $^{14}\text{C}_\text{TC}$	-0.0001	0.0006	0.0027	0.0008	1.0586	0.0016	0.0000	0.0002	1.0675	0.0007	0.5118	0.001										
n	2		3		2		5		3		1											
Loading range ( $\mu\text{g}$ )	700 - 750		60 - 560		730 - 770		740 - 1050		900 - 960		760											
CO <sub>2</sub> isolation & $^{14}\text{C}/^{12}\text{C}$ analysis	Reference material is combusted in 6 mm O.D. quartz tubes with 80 mg CuO for 3 hours at 900°C. Sample-CO <sub>2</sub> is purified cryogenically & reduced to graphite (Xu et al., 2007).																					
<b><math>\delta^{13}\text{C}</math> analysis</b>																						
$\delta^{13}\text{C}_\text{VPDB}$ (‰)	-27.61	0.08	-23.06	0.08	-12.22	0.16	n/a		-26.74	-25.84	0.07											
n	5		5		9		n/a		1		2											
Loading range ( $\mu\text{g}$ or $\mu\text{g C}^*$ )	15 - 70		20 - 50		20		n/a		160		600											
CO <sub>2</sub> isolation	Material is loaded on a quartz filter and combusted in a Sunset OCEC aerosol analyzer ( <a href="http://www.sunlab.com">http://www.sunlab.com</a> ) using the ECT9 method. Sample-CO <sub>2</sub> is collected in a U-shaped flask submerged in liquid N <sub>2</sub> at -196°C (Fig. 1b).						n/a	See description for Regal black, C1150, and sucrose.														
CO <sub>2</sub> extraction & $^{13}\text{C}/^{12}\text{C}$ analysis	Sample-CO <sub>2</sub> is cryogenically purified on a vacuum line and sealed into an ampoule for analysis with a MAT253 Isotopic Ratio Mass Spectrometer (Huang et al., 2013).																					

445 \*Sucrose was loaded as a solution ( $\mu\text{g C}$ ), Regal Black, C1150, Adipic acid, Rice char, and SRM-1649a as a fine powder ( $\mu\text{g dry mass}$ ); n/a = not applicable

**Table 3.** Comparison of the OC and EC ECT9 and Swiss-4S isolation protocols.

Carrier gas	Carbon fraction	Temperature °C	Duration s	Comments
<b>ETC9<sup>a</sup></b>				
He-purge		20 – 50	90	Purging of volatile and semi-volatile OC
He	OC	550	600	
He	PyOC + CC	870	600	Minimizing charred OC contribution to EC
O <sub>2</sub> /He <sup>b</sup>	EC	900	420	
<b>Swiss-4S<sup>c</sup></b>				
O <sub>2</sub> -purge		20 – 50	90	Purging of volatile and semi-volatile OC
O <sub>2</sub>	S1_OC	375	240	
O <sub>2</sub>	S2_OC	475	120	
He	S3_OC	650	180	
O <sub>2</sub>	S4_EC	760	160	Water-soluble OC is removed by water extraction prior to thermal analysis.

450 <sup>a</sup>PyOC + CC = pyrolysis OC + carbonate carbon; <sup>b</sup>The flow of 10% O<sub>2</sub> + 90% He mixing with the flow of 100% He resulting in 2% O<sub>2</sub> + 98% He. in <sup>c</sup>The EC punch is flushed with Milli-Q water prior the analysis to remove the water-soluble OC and minimize charring (Zhang et al., 2012; Mouteva et al., 2015a).

455

**Table 4.** Comparison of the procedural contamination with extraneous carbon for aerosol reference materials partitioned into organic carbon (OC) and elemental carbon (EC) with the ECT9 or Swiss\_4S protocols based on their <sup>14</sup>C contents. We assume a measurement uncertainty of 50% (see Methods).

Contamination Source	ECT9 μg C	Swiss_4S <sup>a</sup>
<b>OC/EC isolation + trapping</b>		
Modern	0.55	0.37
Fossil	0.30	0.13
Total	0.85	0.50
<b><sup>14</sup>C analysis<sup>b</sup></b>		
Modern	0.35	0.43
Fossil	0.10	0.53
Total	0.45	0.97
<b>Full set-up</b>		
Modern	0.90	0.80
Fossil	0.40	0.67
Total	1.30	1.47

460 <sup>a</sup>From Mouteva et al. (2015a), <sup>b</sup>Carbon introduced during sample combustion, CO<sub>2</sub> purification and graphitization, and measurement with <sup>14</sup>C-AMS.

475

## Figure captions

**Figure 1:** Overview of the carbonaceous aerosol analysis system at Environment and Climate Change Canada.

(a) Schematic flow chart for  $^{13}\text{C}$  &  $^{14}\text{C}$  measurements of OC/EC via ECT9, including 1) OC/EC isolation/CO<sub>2</sub> collection via cryo-trapping, 2) CO<sub>2</sub> purification, and 3) isotope analysis with IRMS ( $^{13}\text{C}/^{12}\text{C}$  of CO<sub>2</sub>) or AMS ( $^{13}\text{C}/^{12}\text{C}$  and  $^{14}\text{C}/^{12}\text{C}$  of graphite targets).

(b) Thermogram of the ECT9 protocol on a Sunset OC/EC Analyzer. First, organic carbon (OC) is thermally desorbed at 550°C for 600 seconds in 100% He, then any pyrolyzed OC (PyOC), refractory OC, and carbonate carbon (CC) is released at 870°C in 100% He for 600 seconds. Finally, elemental carbon (EC) is combusted at 900°C for 420 seconds by introducing 2% O<sub>2</sub> in He. All carbon fractions are oxidized to CO<sub>2</sub> followed by reduction to CH<sub>4</sub> and quantification via flame ionization detection (FID) for carbon content or purified and cryo-trapped in Pyrex ampoules for isotope analysis. Example FID signals are shown for a pure OC reference material (sucrose) mixed with a pure EC material (regal black) along with the internal standard (CH<sub>4</sub>).

**Figure 2:** Cross-validation of carbon-mass prepared, isolated by the ECT9 protocol and collected via cryo-trapping at ECCC and then, retrieved during the purification and graphitization on a KCCAMS vacuum line. Carbon fractions (organic carbon (OC), elemental carbon (EC), or total carbon (TC)) were isolated from two reference materials for OC (sucrose, adipic acid), EC (regal black, C1150), and one OC & EC mixture (rice char). Most of the points deviating from the 1:1 line are carbon-rich reference materials, e.g., Regal black and C1150 (>90% TC), which usually there are greater uncertainties in initial mass determination via weighing using microbalance, because their sample sizes aimed were very small.

**Figure 3:** Radiocarbon ( $^{14}\text{C}$ ) compositions, expressed as Fraction Modern Carbon, of total carbon (TC, circles), organic carbon (OC, triangles) and elemental carbon (EC, squares) fractions isolated with the ECT9 protocol from modern or fossil individual reference materials. a) Sucrose and b) adipic acid are modern and fossil OC, respectively, c) regal black and d) C1150 are fossil EC, and e) rice char is a mixture of modern OC and EC. Open and solid symbols represent  $^{14}\text{C}$  data before and after correction for extraneous carbon introduced during OC/EC isolation and subsequent  $^{14}\text{C}$  analysis, respectively. The dashed line indicates the consensus value determined from regular-sized bulk samples of these materials undergoing off-line combustions (see Table 2).

**Figure 4:** Radiocarbon ( $^{14}\text{C}$ ) composition, expressed as Fraction Modern Carbon, of a) organic (OC, triangles) or b) elemental (EC, squares) carbon fractions isolated with the ECT9 protocol from mixtures of pure modern OC (sucrose) with fossil EC (regal black). Open and solid symbols represent  $^{14}\text{C}$  data before and after correction for extraneous carbon introduced during OC/EC isolation via ECT9 and subsequent  $^{14}\text{C}$  analysis via AMS, respectively (see Table S7). The dashed line indicates the consensus value (see Table 2).

**Figure 5:** Radiocarbon ( $^{14}\text{C}$ ) compositions, expressed in fraction modern carbon, of organic (OC, triangles) and elemental (EC, squares) carbon fractions isolated with the ECT9 protocol from the mixtures of reference materials. Fraction of modern carbon a) OC and c) EC isolated from mixtures of pure fossil OC (adipic acid) with modern bulk rice char (made of 14% OC and 86 % EC), and of b) OC and d) EC isolated from mixtures of pure fossil OC (adipic acid) with modern EC from rice char \_EC (rice char \_OC has been removed before mixing). Open and solid

symbols represent data before and after correction for extraneous carbon introduced during OC/EC isolation via ECT9 and subsequent  $^{14}\text{C}$  analysis via AMS respectively (Table S7). The dashed line indicates the consensus value (see Table 2).

515 **Figure 6:** Thermograms of pure or bulk references. **a)** Regal black and **b)** Sucrose and **c)** Rice char. Temperature (blue solid line) and FID signals (integrated yellow area with green line) on the left axes and laser (red solid line) on the right axis. It is observed that on the three thermograms during the temperature stage of 870°C, the laser transmittance signals decrease first and increases again before the next temperatures stage, minimizing  $\text{PyOC}$  fraction, i.e., possible charred OC contribution to EC.

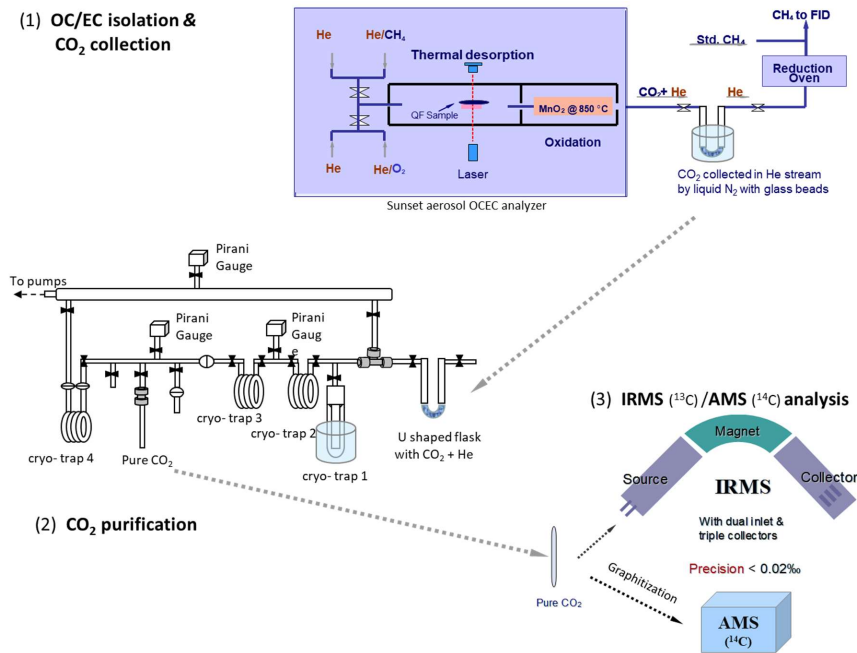
520 **Figure 7:** Thermograms of the filters directly collected from tailpipe exhaust of a diesel engine vehicle in **a)** and a gasoline engine passage car in **b)**. The legends are the same as Fig 6. It is noticed that the mass fraction from the temperature stage of 870°C in **b)** is obvious larger than that in **a)**. The latter is negligible indicating that the amount of  $\text{PyOC}$  fraction is sample-matrix dependent. The amount of  $\text{PyOC}$  from gasoline vehicle emissions is likely larger than that from diesel vehicle emissions. It was noticed that the laser signal reaches the initial value before the 900°C stage for EC releasing, demonstrating that the charring contribution to EC is minimized.

525 **Figure 8:** Thermograms of fine particles (PM1.0  $\mu\text{m}$ ) from the filter samples collected at an Arctic site, i.e., Alert, NU, Canada in summer **a)** and in winter **b)** of 2015. The legends are the same as Fig 6. It is clearly shown on both thermograms that during 550°C stage, the laser signal starts decreasing (implying charred OC formation) and begins increasing during 870°C and reaches the initial value before the EC stage (indicating the contribution to EC by charred OC is minimized or removed).

530 **Figure 9:** Thermograms of the SRM 8785 filters (the fine fraction (PM<sub>2.5</sub>) of re-suspended urban dust particles from SRM 1649a and collected on quartz filters) with various amount of materials ranging from 614 mg to 1723 mg via two different thermal protocols. **a)** and **b)** were obtained by ECT9. The legends are the same as Fig 6. Both thermograms in **a)** and **b)** show the similar patterns as in Fig. 6, 7, 8. that the laser signals reaching the initial value are just before the temperature stage of EC, suggesting that the charred OC contribution to EC is minimized. The thermogram in **c)** is obtained from the same filter in **b)** but by Swiss-4 protocol for comparison. The legends are similar except for the integrated area with green line, which stands for  $\text{CO}_2$  in ppm (by NDIR) instead of FID signals.

540 **Figures**

Figure 1a . Schematic procedures for  $^{13}\text{C}$  &  $^{14}\text{C}$  measurements of OC/EC via ECT9

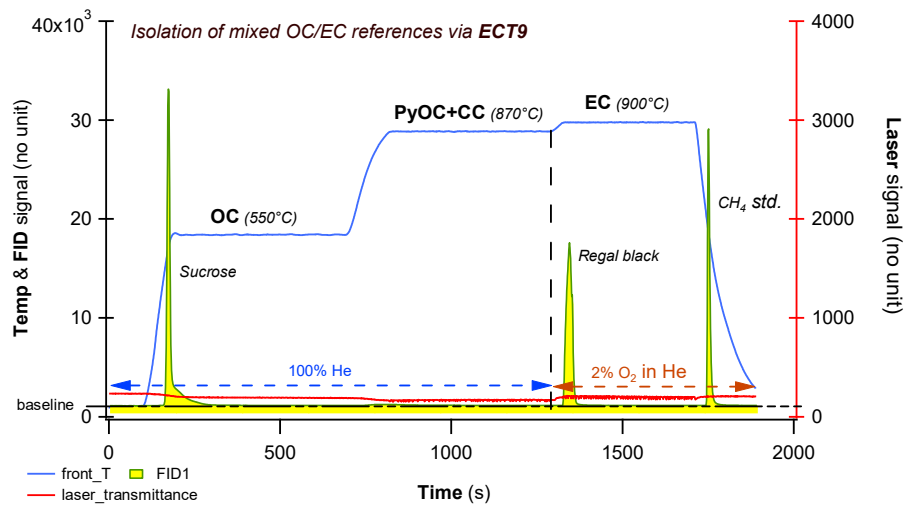


545

550

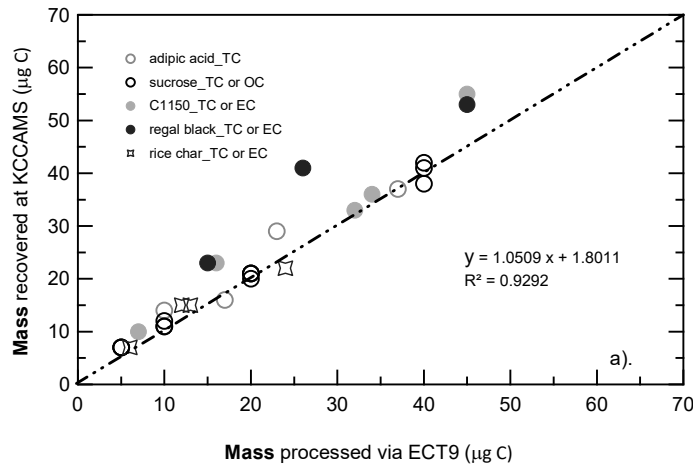
555

560

**Figure 1b**

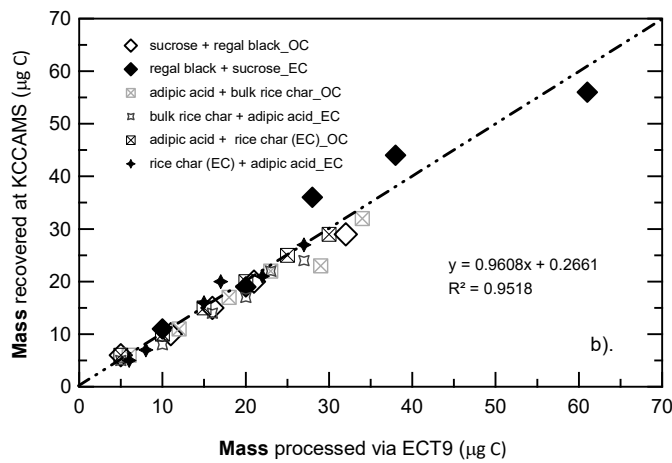
575 **Figure 2**

a)



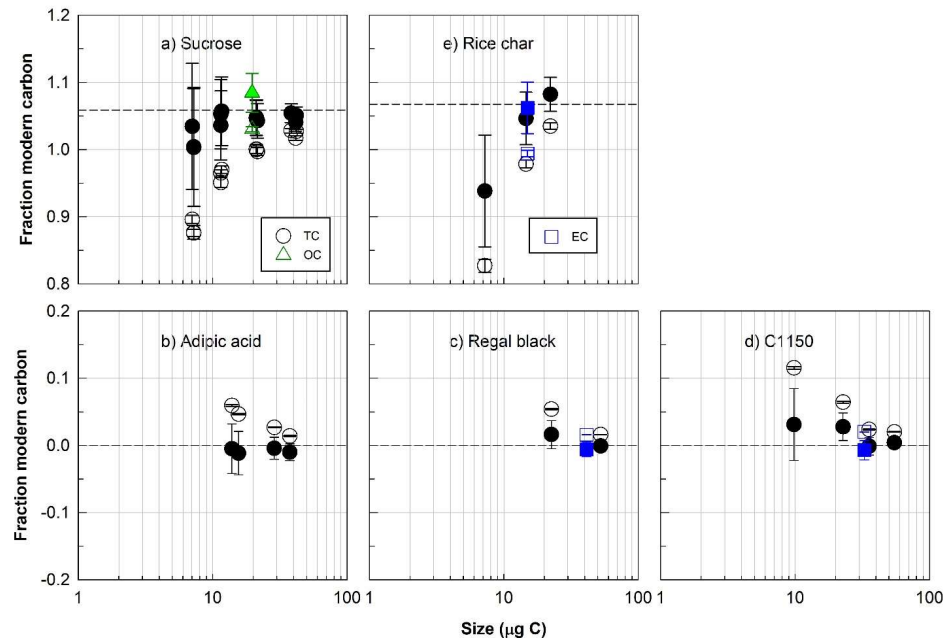
a).

b)



b).

Figure 3



585

590

595

Figure 4

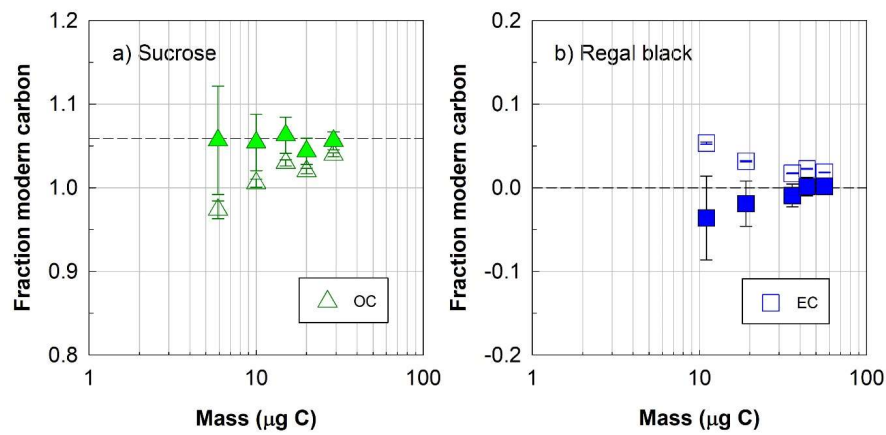


Figure 5

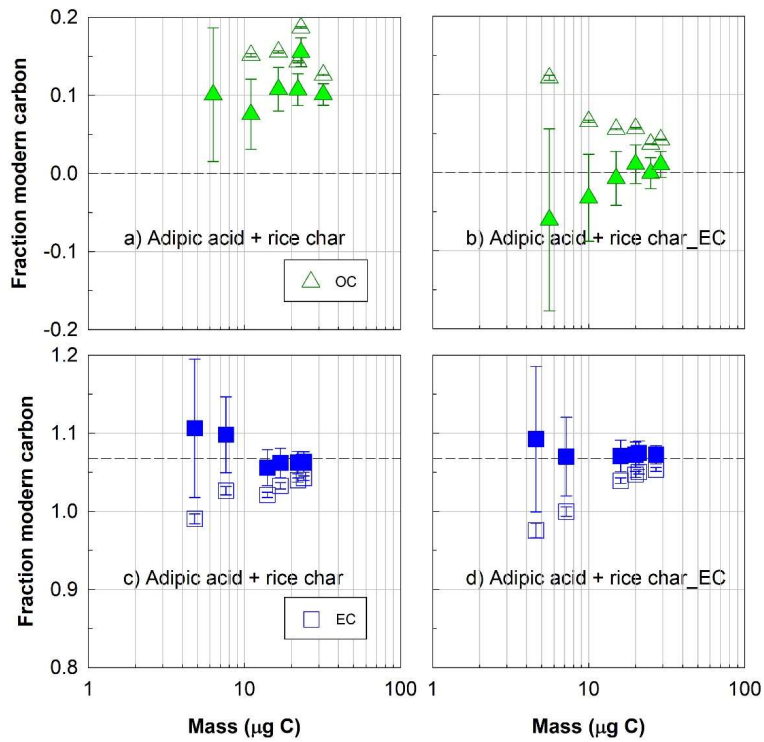
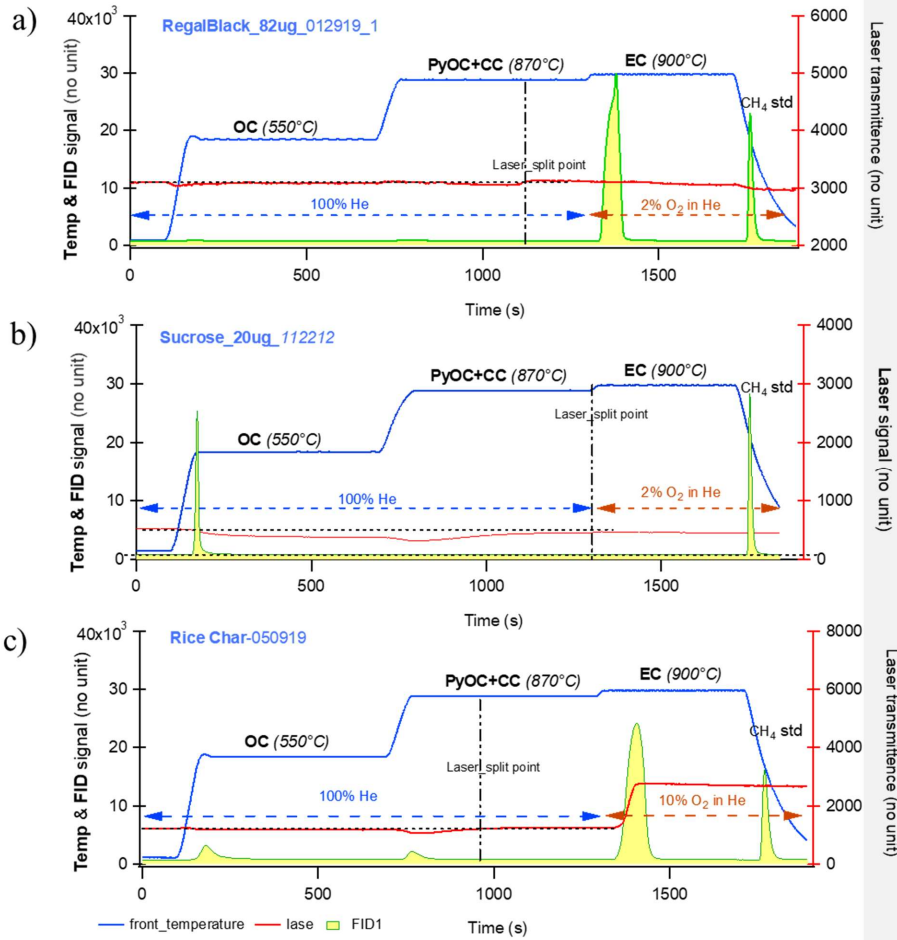


Figure 6



635 Figure 7

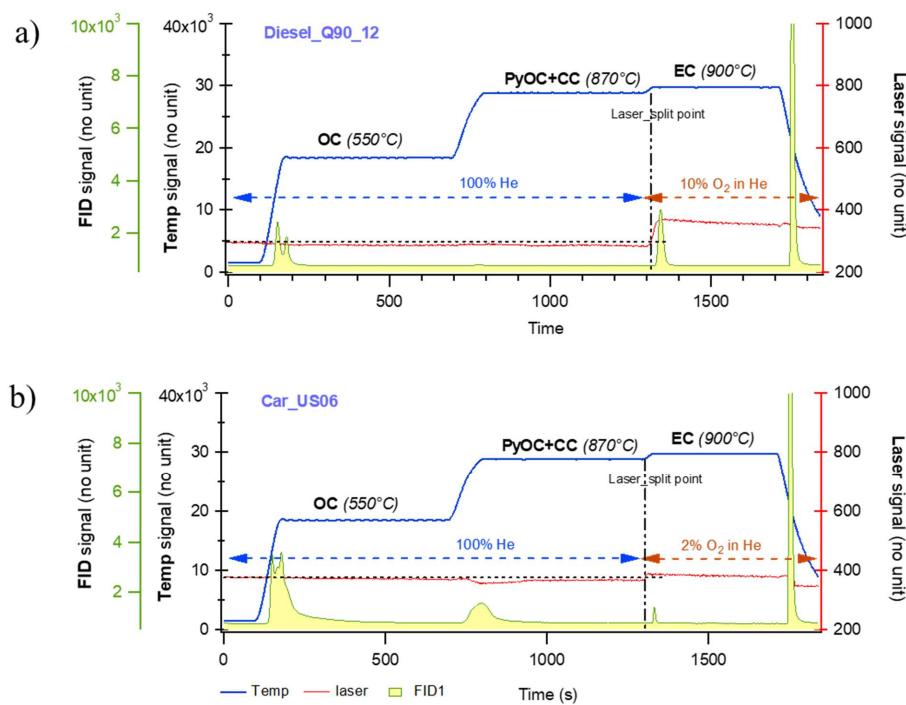
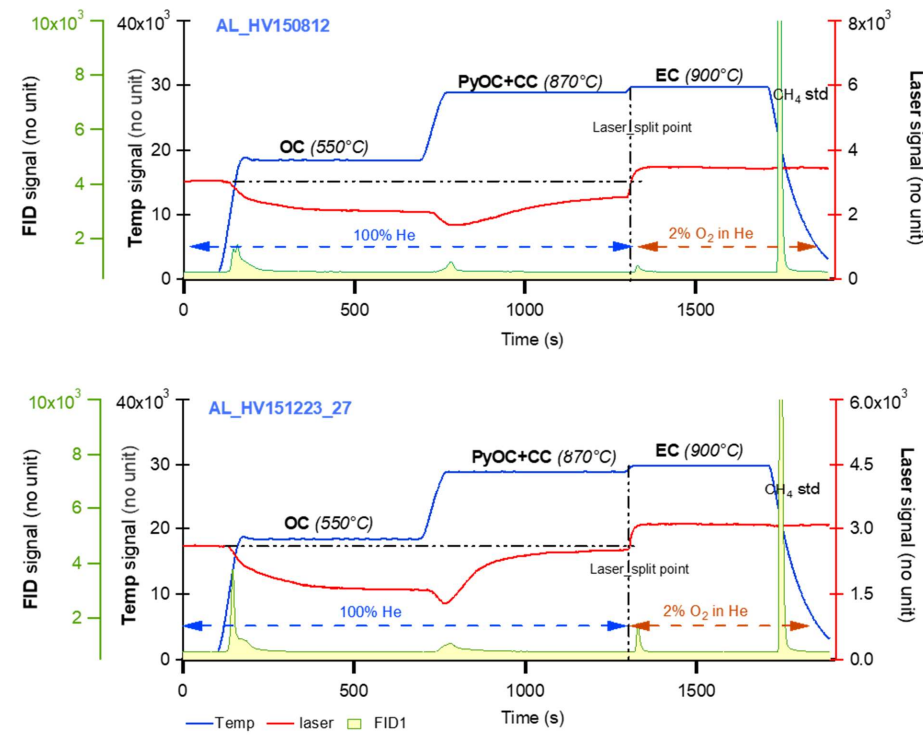


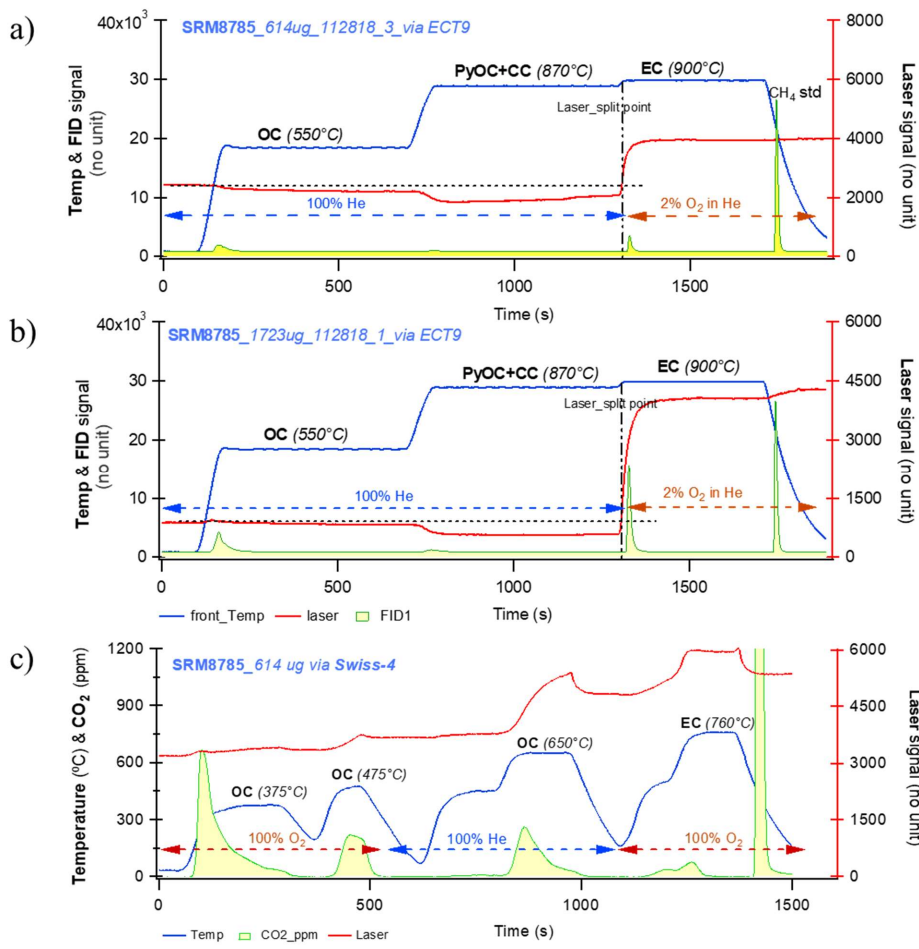
Figure 8



650

655

Figure 9



## References

Andersson, A., Deng, J., Du, K., Zheng, M., Yan, C., Sköld, M. and Gustafsson, Ö.: Regionally-Varying Combustion Sources of the January 2013 Severe Haze Events over Eastern China, *Environ. Sci. Technol.*, 49(4), 2038–2043, doi:10.1021/es503855e, 2015.

665 Barrett, T. E., Robinson, E. M., Usenko, S. and Sheesley, R. J.: Source Contributions to Wintertime Elemental and Organic Carbon in the Western Arctic Based on Radiocarbon and Tracer Apportionment, *Environ. Sci. Technol.*, 49(19), 11631–11639, doi:10.1021/acs.est.5b03081, 2015.

Beverly, R. K., Beaumont, W., Tauz, D., Ormsby, K. M., Reden, K. F. Von, Santos, G. M. and Sounthor, J. R.: The 670 Keck Carbon Cycle AMS laboratory, University of California, Irvine: Status report, *Radiocarbon*, 52(2), 301–309, 2010.

Birch, M. E.: Applied Occupational and Environmental Hygiene Occupational Monitoring of Particulate Diesel Exhaust by NIOSH Method 5040, *Appl. Occup. Environ. Hyg.*, 17(6), 400–405, doi:10.1080/10473220290035390 To, 2002.

675 Bond, T. C., Doherty, S. J., Fahey, D. W., Forster, P. M., Berntsen, T., DeAngelo, B. J., Flanner, M. G., Ghan, S., Kärcher, B., Koch, D., Kinne, S., Kondo, Y., Quinn, P. K., Sarofim, M. C., Schultz, M. G., Schulz, M., Venkataraman, C., Zhang, H., Zhang, S., Bellouin, N., Guttikunda, S. K., Hopke, P. K., Jacobson, M. Z., Kaiser, J. W., Klimont, Z., Lohmann, U., Schwarz, J. P., Shindell, D., Storelvmo, T., Warren, S. G. and Zender, C. S.: Bounding the role of black carbon in the climate system: A scientific assessment, *J. Geophys. Res. Atmos.*, 118(11), 5380–5552, 2013.

680 Cavalli, F., Viana, M., Yttri, K. E., Genberg, J. and Putaud, J.: Toward a standardised thermal-optical protocol for measuring atmospheric organic and elemental carbon : the EUSAAR protocol, , 79–89, 2010.

Chan, T. W., Huang, L., Leaitch, W. R., Sharma, S., Brook, J. R., Slowik, J. G., Abbatt, J. P. D., Brickell, P. C., Liggio, J., Li, S. M. and Moosmüller, H.: Observations of OM/OC and specific attenuation coefficients (SAC) in 685 ambient fine PM at a rural site in central Ontario, Canada, *Atmos. Chem. Phys.*, 10(5), 2393–2411, doi:10.5194/acp-10-2393-2010, 2010.

Chan, T., Meloche, E., Kubsh, J., Brezny, R. et al.: Impact of Ambient Temperature on Gaseous and Particle Emissions from a Direct Injection Gasoline Vehicle and its Implications on Particle Filtration, *SAE Int. J. Fuels Lubr.* 6(2):350-371, [doi.org/10.4271/2013-01-0527](https://doi.org/10.4271/2013-01-0527), 2013.

690 Chan, T. W., Huang, L., Banwait, K., Zhang, W., Ernst, D., Wang, X., John, G., Chow, J. C., Green, M., Czimczik, C. I., Santos, G. M. and Sharma, S.: Inter-comparison of the Elemental and Organic Carbon Mass Measurements from Three North American National Long-term Monitoring Networks, *Atmos. Meas. Tech.*, 12, 4543–4560, 2019 , <https://doi.org/10.5194/amt-12-4543-2019>.

Chow, J. C., Watson, J. G., Crow, D., Lowenthal, D. H. and Merrifield, T.: Comparison of IMPROVE and NIOSH 695 Carbon Measurements, *Aerosol Sci. Technol.*, 34(1), 23–34, 2001.

**Commented [CC8]:** It appears that the text starts too far to the left. Check alignment.

Chow, J. C., Watson, J. G., Chen, L. W. A., Arnott, W. P., Moosmüller, H. and Fung, K.: Equivalence of elemental carbon by thermal/optical reflectance and transmittance with different temperature protocols, *Environ. Sci. Technol.*, 38(16), 4414–4422, doi:10.1021/es034936u, 2004.

Cohen, A. J., Brauer, M., Burnett, R., Anderson, H. R., Frostad, J., Estep, K., Balakrishnan, K., Brunekreef, B.,  
700 Dandona, L., Dandona, R., Feigin, V., Freedman, G., Hubbell, B., Jobling, A., Kan, H., Knibbs, L., Liu, Y.,  
Martin, R., Morawska, L., Pope, C. A., Shin, H., Straif, K., Shaddick, G., Thomas, M., van Dingenen, R., van  
Donkelaar, A., Vos, T., Murray, C. J. L. and Forouzanfar, M. H.: Estimates and 25-year trends of the global  
burden of disease attributable to ambient air pollution: an analysis of data from the Global Burden of Diseases  
Study 2015, *Lancet*, 389(10082), 1907–1918, doi:10.1016/S0140-6736(17)30505-6, 2017.

705 Currie, L. A., Benner, B. A. J., Kessler, J. D., Klinedinst, D. B., Klouda, G. A., Marolf, J. V., Slater, J. F., Wise, S.  
A., Cachier, H., Cary, R., Chow, J. C., Watson, J., Druffel, E. R. M., Masiello, C. A., Eglinton, T. I., Pearson, A.,  
Reddy, C. M., Gustafsson, Ö., Quinn, J. G., Hartmann, P. C., Hedges, J. I., Prentice, K. M., Kirchstetter, T. W.,  
Novakov, T., Puxbaum, H. and Schmid, H.: A Critical Evaluation of Interlaboratory Data on Total, Elemental,  
and Isotopic Carbon in the Carbonaceous Particle Reference Material, NIST SRM 1649a, *J. Res. Natl. Inst. Stand.*  
710 *Technol.*, 107(3), 279–298, 2002.

Després, V. R., Alex Huffman, J., Burrows, S. M., Hoose, C., Safatov, A. S., Buryak, G., Fröhlich-Nowoisky, J.,  
Elbert, W., Andreae, M. O., Pöschl, U. and Jaenicke, R.: Primary biological aerosol particles in the atmosphere: A  
review, *Tellus, Ser. B Chem. Phys. Meteorol.*, 64(1), 15598, doi:10.3402/tellusb.v64i0.15598, 2012.

Eckhardt, S., B. Quennehen,a D. J. L. Olivié, T. K. Berntsen, R. Cherian, J. H. Christensen, W. Collins, S.  
715 Crepinsek, N. Daskalakis, M. Flanner, A. Herber, C. Heyes, Ø. Hodnebrog, L. Huang, M. Kanakidou, Z. Klimont,  
J. Langner, K. S. Law, M. T. Lund, R. Mahmood, A. Massling, S. Myriokefalitakis, I. E. Nielsen, J. K. Nøgaard,  
J. Quaas, P. K. Quinn, J.-C. Raut, S. T. Rumbold, M. Schulz, S. Sharma, R. B. Skeie, H. Skov, T. Uttal, K. von  
Salzen, and A. Stohl. Current model capabilities for simulating black carbon and sulfate concentrations in the  
Arctic atmosphere: a multi-model evaluation using a comprehensive measurement data set, *Atmos. Chem. Phys.*,  
720 15, 9413–9433, 2015 [www.atmos-chem-phys.net/15/9413/2015/](http://www.atmos-chem-phys.net/15/9413/2015/) doi:10.5194/acp-15-9413-2015

Fuzzi, S., Baltensperger, U., Carslaw, K., Decesari, S., Denier Van Der Gon, H., Facchini, M. C., Fowler, D., Koren,  
I., Langford, B., Lohmann, U., Nemitz, E., Pandis, S., Riipinen, I., Rudich, Y., Schaap, M., Slowik, J. G.,  
Spracklen, D. V., Vignati, E., Wild, M., Williams, M. and Gilardoni, S.: Particulate matter, air quality and  
climate: Lessons learned and future needs, *Atmos. Chem. Phys.*, 15(14), 8217–8299, doi:10.5194/acp-15-8217-  
725 2015, 2015.

Grahame, T. J., Klemm, R., Schlesinger, R. B., Gwen Eklund, A., Chow, J. C., Greenbaum, D. S., Hidy, G. M.,  
Kleinman, M. T., Watson, J. G., Wyzga, R. E., Grahame, T. J., Klemm, R. and Schlesinger, R. B.: Public health  
and components of particulate matter: The changing assessment of black carbon, *J. Air Waste Manag. Assoc.*,  
64(11), 1221–1231, doi:10.1080/10962247.2014.960218, 2014.

730 Graven, H. D.: Impact of fossil fuel emissions on atmospheric radiocarbon and various applications of radiocarbon

over this century, Proc. Natl. Acad. Sci., 112(31), 9542–9545, doi:10.1073/pnas.1504467112, 2015.

Graven, H., Keeling, R. F., & Rogelj, J. (2020). Changes to Carbon Isotopes in Atmospheric CO<sub>2</sub> over the Industrial Era and into the Future. *Global biogeochemical cycles*, 34(11), e2019GB006170.

Hallquist, M., Wenger, J. C., Baltensperger, U., Rudich, Y., Simpson, D., Claeys, M., Dommen, J., Donahue, N. M.,  
 735 George, C., Goldstein, A. H., Hamilton, J. F., Herrmann, H., Hoffmann, T., Iinuma, Y., Jang, M., Jenkin, M. E., Jimenez, J. L., Kiendler-Scharr, A., Maenhaut, W., McFiggans, G., Mentel, T. F., Monod, A., Prévôt, A. S. H., Seinfeld, J. H., Surratt, J. D., Szmigielski, R. and Wildt, J.: The formation, properties and impact of secondary organic aerosol: current and emerging issues, *Atmos. Chem. Phys.*, 9, 5155–5236, 2009.

Hand, J. L., B. A. Schichtel, W. C. Malm, and N. H. Frank, Spatial and Temporal Trends in PM2.5 Organic and  
 740 Elemental Carbon across the United States, *Advances in Meteorology*

Volume 2013, Article ID 367674, 13 pages <http://dx.doi.org/10.1155/2013/367674>.

Hammes, K., Smernik, R. J., Skjemstad, J. O., Herzog, A., Vogt, U. F. and Schmidt, M. W. I.: Synthesis and characterisation of laboratory-charred grass straw (*Oryza sativa*) and chestnut wood (*Castanea sativa*) as reference materials for black carbon quantification, *Org. Geochem.*, 37(11), 1629–1633,  
 745 doi:10.1016/j.orggeochem.2006.07.003, 2006.

Hammes, K., Schmidt, M. W. I., Smernik, R. J., Currie, L. A., Ball, W. P., Nguyen, T. H., Louchouarn, P., Houel, S. Elmqvist, M., Cornelissen, G., Skjemstad, J. O., Dunn, J. C., Hatcher, P. G., Hockaday, W. C., Smith, D. M., Hartkopf-fro, C., Bo, A., Gschwend, P. M., Flores-cervantes, D. X., Largeau, C., Rumpel, C., Guggenberger, G., Kaiser, K., Rosa, M. De, Manning, D. A. C. and Lo, E.: Comparison of quantification methods to measure fire-derived ( black / elemental ) carbon in soils and sediments using reference materials from soil , water , sediment and the atmosphere, 21, doi:10.1029/2006GB002914, 2007.

Hammes, K., Smernik, R. J., Skjemstad, J. O. and Schmidt, M. W. I.: Characterisation and evaluation of reference materials for black carbon analysis using elemental composition , colour , BET surface area and C NMR spectroscopy, *Appl. Geochemistry*, 23, 2113–2122, doi:10.1016/j.apgeochem.2008.04.023, 2008.

750 Heal, M. R.: The application of carbon-14 analyses to the source apportionment of atmospheric carbonaceous particulate matter: A review, *Anal. Bioanal. Chem.*, 406(1), 81–98, doi:10.1007/s00216-013-7404-1, 2014.

Huang, L., The issue of harmonizing the methodologies for emission inventories of GHGs with those of SLCFs, presentation at the IPCC Expert Meeting on SLCFs, Geneva, May, 2018 ([https://www.ipcc-nccip.iges.or.jp/public/mtdocs/1805\\_Geneva.html](https://www.ipcc-nccip.iges.or.jp/public/mtdocs/1805_Geneva.html) )

760 Huang, L., Brook, J. R., Zhang, W., Li, S. M., Graham, L., Ernst, D., Chivulescu, A. and Lu, G.: Stable isotope measurements of carbon fractions (OC/EC) in airborne particulate: A new dimension for source characterization and apportionment, *Atmos. Environ.*, 40(15), 2690–2705, doi:10.1016/j.atmosenv.2005.11.062, 2006.

Huang, L., Gong, S. L., Sharma, S., Lavoué, D. and Jia, C. Q.: A trajectory analysis of atmospheric transport of black carbon aerosols to Canadian high Arctic in winter and spring (1990–2005), *Atmos. Chem. Phys.*, 10(11),  
 765 5065–5073, doi:10.5194/acp-10-5065-2010, 2010.

Irei, S., Laboratory study of stable carbon isotope ratio of secondary particulate organic matter in the gas-phase, PhD thesis, York University, Sept. 2008.

Janssen, N. A., Gerlofs-Nijland, M. E., Lanki, T., Salonen, R. O., Cassee, F., Hoek, G., Fischer, P., Brunekreef, B. and Krzyzanowski, M.: Health effects of black carbon, WHO Regional Office for Europe, Copenhagen, Denmark., 2012.

Jimenez, J. L., Canagaratna, M. R., Donahue, N. M., Prevot, a. S. H., Zhang, Q., Kroll, J. H., DeCarlo, P. F., Allan, J. D., Coe, H., Ng, N. L., Aiken, a. C., Docherty, K. S., Ulbrich, I. M., Grieshop, A. P., Robinson, a. L., Duplissy, J., Smith, J. D., Wilson, K. R., Lanz, V. a., Hueglin, C., Sun, Y. L., Tian, J., Laaksonen, A., Raatikainen, T., Rautiainen, J., Vaattovaara, P., Ehn, M., Kulmala, M., Tomlinson, J. M., Collins, D. R., Cubison, M. J., Dunlea, E. J., Huffman, J. A., Onasch, T. B., Alfarra, M. R., Williams, P. I., Bower, K., Kondo, Y., Schneider, J., Drewnick, F., Borrmann, S., Weimer, S., Demerjian, K., Salcedo, D., Cottrell, L., Griffin, R., Takami, A., Miyoshi, T., Hatakeyama, S., Shimono, A., Sun, J. Y., Zhang, Y. M., Dzepina, K., Kimmel, J. R., Sueper, D., Jayne, J. T., Herndon, S. C., Trimborn, a. M., Williams, L. R., Wood, E. C., Middlebrook, A. M., Kolb, C. E., Baltensperger, U., Worsnop, D. R., Dunlea, J., Huffman, J. A., Onasch, T. B., Alfarra, M. R., Williams, P. I., Bower, K., Kondo, Y., Schneider, J., Drewnick, F., Borrmann, S., Weimer, S., Demerjian, K., Salcedo, D., Cottrell, L., Griffin, R., Takami, A., Miyoshi, T., Hatakeyama, S., Shimono, A., Sun, J. Y., Zhang, Y. M., Dzepina, K., Kimmel, J. R., Sueper, D., Jayne, J. T., Herndon, S. C., Trimborn, a. M., Williams, L. R., Wood, E. C., Middlebrook, A. M., Kolb, C. E., Baltensperger, U., Worsnop, D. R., Dunlea, E. J., Huffman, J. A., et al.: Evolution of organic aerosols in the atmosphere, *Science* (80-), 326(5959), 1525–1529, doi:10.1126/science.1180353, 2009.

Kanakidou, M., Seinfeld, J. H., Pandis, S. N., Barnes, I., Dentener, F. J., Facchini, M. C., Van Dingenen, R., Ervens, B., Nenes, A., Nielsen, C. J., Swietlicki, E., Putaud, J. P., Balkanski, Y., Fuzzi, S., Horth, J., Moortgat, G. K., Winterhalter, R., Myhre, C. E. L., Tsigaridis, K., Vignati, E., Stephanou, E. G. and Wilson, J.: Organic aerosol and global climate modelling: a review, *Atmos. Chem. Phys.*, 5(4), 1053–1123, doi:10.5194/acp-5-1053-2005, 2005.

Klouda, G., Filliben, J., Parish, H., Chow, J., Watson, J. and Cary, R.: Reference Material 8785: air particulate matter on filter media, *Aerosol Sci. Technol.*, 39(2), 173–183, 2005.

Laskin, A., Laskin, J. and Nizkorodov, S. A.: Chemistry of Atmospheric Brown Carbon, *Chem. Rev.*, 115(10), 4335–4382, doi:10.1021/cr5006167, 2015.

Levin, I., Naegler, T., Kromer, B., Diehl, M., Francey, R. J., Gomez-Pelaez, A. J., Steele, L. P., Wagenbach, D., Weller, R., Worthy, D. E. and Deihl, M.: Observations and modelling of the global distribution and long-term trend of atmospheric  $^{14}\text{CO}_2$ , *Tellus B*, 62, 26–46, 2010.

Meredith, W., P. L. Ascough, M. I. Bird, D. J. Large, C.E. Snape, Y. Sun, E. L. Tilston, Assessment of hydprprolysis as a method for the qualification of black carbon using standard reference materials, *Geochem. Cosmochim. Acta* 97, 131-147, 2012.

Mouteva, G. O., Fahrni, S. M., Santos, G. M., Randerson, J. T., Zhang, Y.-L., Szidat, S. and Czimczik, C. I.:  
Accuracy and precision of  $^{14}\text{C}$ -based source apportionment of organic and elemental carbon in aerosols using the  
Swiss\_4S protocol, *Atmos. Meas. Tech.*, 8(9), 3729–3743, doi:10.5194/amt-8-3729-2015, 2015a.

Mouteva, G. O., Czimczik, C. I., Fahrni, S. M., Wiggins, E. B., Rogers, B. M., Veraverbeke, S., Xu, X., Santos, G.  
805 M., Henderson, J., Miller, C. E. and Randerson, J. T.: Black carbon aerosol dynamics and isotopic composition in  
Alaska linked with boreal fire emissions and depth of burn in organic soils, *Global Biogeochem. Cycles*, 29(11),  
1977–2000, doi:10.1002/2015GB005247, 2015b.

Pöschl, U.: Atmospheric aerosols: Composition, transformation, climate and health effects, *Angew. Chemie - Int.*  
Ed., 44(46), 7520–7540, doi:10.1002/anie.200501122, 2005.

810 Putaud, J. P., Van Dingenen, R., Alastuey, A., Bauer, H., Birmili, W., Cyrys, J., Flentje, H., Fuzzi, S., Gehrig, R.,  
Hansson, H. C., Harrison, R. M., Herrmann, H., Hitzenberger, R., Hüglin, C., Jones, A. M., Kasper-Giebl, A.,  
Kiss, G., Kousa, A., Kuhlbusch, T. A. J., Löschau, G., Maenhaut, W., Molnar, A., Moreno, T., Pekkanen, J.,  
Perrino, C., Pitz, M., Puxbaum, H., Querol, X., Rodriguez, S., Salma, I., Schwarz, J., Smolik, J., Schneider, J.,  
Spindler, G., ten Brink, H., Tursic, J., Viana, M., Wiedensohler, A. and Raes, F.: A European aerosol  
815 phenomenology - 3: Physical and chemical characteristics of particulate matter from 60 rural, urban, and kerbside  
sites across Europe, *Atmos. Environ.*, 44(10), 1308–1320, doi:10.1016/j.atmosenv.2009.12.011, 2010.

Ridley, D.A., C.L. Heald, K.J. Ridley and J. H. Kroll, Cause and consequences of decreasing atmospheric organic  
aerosol in the United States, *Proc Natl Acad Sci USA*, January 9, 2018 115 (2) 290-295,  
<https://doi.org/10.1073/pnas.1700387115>

820 Leaitch, W.R., L. M. Russell, J. Liu, F. Kolonjari, D. Toom, L. Huang, S. Sharma, . Chivulescu, D. Veber, W.  
Zhang, Organic Functional Groups in the Submicron Aerosol at 82.5°N from 2012 to 2014, *Atmos. Chem. Phys.*,  
18, 3269–3287, 2018

Leaitch, W.R., S. Sharma, L. Huang, D. Toom-Sauntry, A. Chivulescu, A. Marie Macdonald, K. von Salzen, J. R.  
825 Pierce, A. K. Bertram, J. C. Schroder, N. C. Shantz, R. Y.-W. Chang, A.-L. Norman, 2013. Dimethyl sulfide  
control of the clean summertime Arctic aerosol and cloud, *Elementa: Science of the Anthropocene* • 1: 000017 •  
doi: 10.12952/journal.elementa.000017.

[Reimer, P. J., Brown, T. A., & Reimer, R. W., 2004, Discussion: Reporting and calibration of post bomb  \$^{14}\text{C}\$  data,](https://doi.org/10.1080/00222496.2004.9628401)  
[RadioCarbon, V 46, Nr 3, 2004, 1299–1304.](https://doi.org/10.1080/00222496.2004.9628401)

Sharma, S., W. R. Leaitch, L. Huang, D. Veber, F. Kolonjari, W. Zhang, S. J. Hanna, A. K. Bertram, and J. A.  
830 Ogren, 2017. An evaluation of three methods for measuring black carbon in Alert, Canada, *Atmos. Chem. Phys.*,  
17, 15225–15243, 2017 <https://doi.org/10.5194/acp-17-15225-2017>.

Santos, G. M., Moore, R. B., Sounthor, J. R., Griffin, S., Hinger, E. and Zhang, D.: AMS 14C Sample Preparation at  
the KCCAMS/UCI Facility: Status Report and Performance of Small Samples, *Radiocarbon*, 49(2), 255–269,  
doi:10.2458/azu\_js\_rc.49.2925, 2007a.

835 Santos, G. M., Sounthor, J. R., Griffin, S., Beaupre, S. R. and Druffel, E. R. M.: Ultra small-mass AMS  $^{14}\text{C}$  sample preparation and analyses at KCCAMS/UCI Facility, *Nucl. Instruments Methods Phys. Res. Sect. B Beam Interact. with Mater. Atoms*, 259, 293–302, 2007b.

Santos, G. M., Sounthor, J. R., Drenzek, N. J., Ziolkowski, L. A., Druffel, E. R. M., Xu, X., Zhang, D., Trumbore, S. E., Eglinton, T. I. and Hughen, K. A.: Blank assessment for ultra-small radiocarbon samples, *Radiocarbon*, 52, 840 1322–1335, 2010.

Sharma, S., Richard Leitch, W., Huang, L., Veber, D., Kolonjari, F., Zhang, W., Hanna, S. J., Bertram, A. K. and Ogren, J. A.: An evaluation of three methods for measuring black carbon in Alert, Canada, *Atmos. Chem. Phys.*, 17(24), 15225–15243, doi:10.5194/acp-17-15225-2017, 2017.

Shrivastava, M., Cappa, C.D., Fan, J., Goldstein, A.H., Guenther, A.B., Jimenez, J.L., Kuang, C., Laskin, A., 845 Martin, S.T., Ng, N.L. and Petaja, T.: Recent advances in understanding secondary organic aerosol: Implications for global climate forcing. *Reviews of Geophysics*, 55(2), 509-559, 2017.

Stuiver, M. and Polach, H. A.: Discussion Reporting of  $^{14}\text{C}$  Data, *Radiocarbon*, 19(03), 355–363, doi:10.1017/S0033822200003672, 1977.

Szidat, S., Jenk, T. M., Gaggeler, H. W., Synal, H.-A., Hajdas, I., Bonani, G., and Saurer, M.: THEODORE, a two-step heating system for the EC/OC determination of radiocarbon ( $^{14}\text{C}$ ) in the environment, *Nucl. Instrum. Methods B*, 223–224, 850 829–836, 2004

Szidat, S., Jenk, T. M., Synal, H.-A., Kalberer, M., Wacker, L., Hajdas, I., Kasper-Giebl, A. and Baltensperger, U.: Contributions of fossil fuel, biomass-burning, and biogenic emissions to carbonaceous aerosols in Zurich as traced by  $^{14}\text{C}$ , *J. Geophys. Res.*, 111(D7), D07206, 2006.

855 Trumbore, S. E., Sierra, C. A. and Hicks Pries, C. E.: Radiocarbon Nomenclature, Theory, Models, and Interpretation: Measuring Age, Determining Cycling Rates, and Tracing Source Pools, in *Radiocarbon and Climate Change: Mechanisms, Applications and Laboratory Techniques*, edited by E. A. G. Schuur, E. Druffel, and S. E. Trumbore, pp. 45–82, Springer International Publishing, Cham., 2016.

Watson, J. G., Chen, L. A., Chang, O., Chow, J. C., Watson, J. G., Chen, L. A., Chang, M. C. O., Robinson, N. F., 860 Trimble, D. and Kohl, S.: The IMPROVE \_ A Temperature Protocol for Thermal / Optical Carbon Analysis : Maintaining Consistency with a Long-Term Database, *Air Waste Manag.*, 57, 1014–1023, doi:10.3155/1047-3289.57.9.1014, 2007.

Wex, H., Huang, L., Zhang, W., Huang, H., Traversi, R., Becagli, S., Sheesley, R.J., Moffett, C. E., Barrett, T.E., 865 Bossi, R., Skov, H., Hunerber, A., Lubitz, J., Loffler, M., Linke, O., Hartmann, M., Herenz, P., and Stratmann, F.: Annual variability of ice nucleating particle concentrations at different Arctic locations , *Atmos. Chem. Phys.*, 19, 5293-5311, 2019.

Wiggins, E. B., Czimczik, C. I., Santos, G. M., Chen, Y., Xu, X., Holden, S. R., Randerson, J. T., Harvey, C. F., Kai, F. M. and Yu, L. E.: Smoke radiocarbon measurements from Indonesian fires provide evidence for burning

of millennia-aged peat, *Proc. Natl. Acad. Sci.*, 115(49), 12419–12424, doi:10.1073/pnas.1806003115, 2018.

870 Willis, M. D., Healy, R. M., Riemer, N., West, M., Wang, J. M., Jeong, C., Wenger, J. C., Evans, G. J., Abbatt, J. P. D. and Lee, A. K. Y.: Quantification of black carbon mixing state from traffic : implications for aerosol optical properties , 4693–4706, doi:10.5194/acp-16-4693-2016, 2016.

Winiger, P., Andersson, A., Eckhardt, S., Stohl, A. and Gustafsson, O.: The sources of atmospheric black carbon at a European gateway to the Arctic, *Nat. Commun.*, 7, doi:10.1038/ncomms12776, 2016.

875 Winiger, P., Andersson, A., Eckhardt, S., Stohl, A., Semiletov, I. P., Dudarev, O. V., Charkin, A., Shakhova, N., Klimont, Z., Heyes, C. and Gustafsson, Ö.: Siberian Arctic black carbon sources constrained by model and observation, *Proc. Natl. Acad. Sci.*, 114(7), E1054–E1061, doi:10.1073/pnas.1613401114, 2017.

Winiger, P., T. E. Barrett, R. J. Sheesley, L. Huang, S. Sharma, L. A. Barrie, K. E. Yttri, N. Evangelou, S. Eckhardt, A. Stohl, Z. Klimont, C. Heyes, I. P. Semiletov, O. V. Dudarev, A. Charkin, N. Shakhova, H.

880 Holmstrand, A. Andersson, Ö. Gustafsson, Source apportionment of circum-Arctic atmospheric black carbon from isotopes and modeling. *Sci. Adv.* 2019;5: eaau8052

Xu, J., Martin, R. V., Morrow, A., Sharma, S., Huang, L., Leaitch, W. R., Burkart, J., Schulz, H., Zanatta, M., Willis, M. D., Henze, D. K., Lee, C. J., Herber, A. B. and Abbatt, J. P. D.: Source attribution of Arctic black carbon constrained by aircraft and surface measurements , 11971–11989, 2017.

885 Xu, X., Trumbore, S. E., Zheng, S., Sounthor, J. R., McDuffee, K. E., Luttgen, M. and Liu, J. C.: Modifying a sealed tube zinc reduction method for preparation of AMS graphite targets: Reducing background and attaining high precision, *Nucl. Instruments Methods Phys. Res. Sect. B Beam Interact. with Mater. Atoms*, 259(1), 320–329, doi:10.1016/j.nimb.2007.01.175, 2007.

Yang, F., Huang, L., Duan, F., Zhang, W., He, K., Ma, Y., Brook, J. R., Tan, J., Zhao, Q. and Cheng, Y.:

890 Carbonaceous species in PM2.5 at a pair of rural/urban sites in Beijing, 2005-2008, *Atmos. Chem. Phys.*, 11(15), 7893–7903, doi:10.5194/acp-11-7893-2011, 2011.

Yang, F., J. Tan, Q. Zhao, Z. Du, K. He, Y. Ma, F. Duan, G. Chen, and Q. Zhao, Characteristics of PM2.5 speciation in representative megacities and across China, *Atmos. Chem. Phys.*, *Atmos. Chem. Phys.*, 11, 5207–5219, 2011 [www.atmos-chem-phys.net/11/5207/2011/](http://www.atmos-chem-phys.net/11/5207/2011/) doi:10.5194/acp-11-5207-2011.

895 Zencak, Z., Elmquist, M. and Gustafsson, Ö.: Quantification and radiocarbon source apportionment of black carbon in atmospheric aerosols using the CTO-375 method, *Atmos. Environ.*, 41, 7895–7906, 2007.

Zhang, X., Li, J., Mo, Y., Shen, C., Ding, P., Wang, N., Zhu, S., Cheng, Z., He, J., Tian, Y., Gao, S., Zhou, Q., Tian, C., Chen, Y. and Zhang, G.: Isolation and radiocarbon analysis of elemental carbon in atmospheric aerosols using hydrolysis, *Atmos. Environ.*, 198(August 2018), 381–386, doi:10.1016/j.atmosenv.2018.11.005, 2019.

900 Zhang, X. Y., Wang, Y. Q., Zhang, X. C., Guo, W. and Gong, S. L.: Carbonaceous aerosol composition over various regions of China during 2006, *J. Geophys. Res.*, 113, D14111, 2008.

Zhang, Y. L., Perron, N., Ciobanu, V. G., Zotter, P., Minguillón, M. C., Wacker, L., Prévôt, A. S. H., Baltensperger, U. and Szidat, S.: On the isolation of OC and EC and the optimal strategy of radiocarbon-based source apportionment of carbonaceous aerosols, *Atmos. Chem. Phys.*, 12, 10841–10856, 2012.

905

**Supplementary Information**

**Table S1.** Individual measurements of OC and EC via ECT9 at ECCC for the references listed in Table 1.

Lab ID	Date	<sup>a</sup> Loaded mass on filter	Carbon fraction			OC <sub>total</sub> /TC	EC/TC	TC/loaded mass
			OC	P <sub>OC+CC</sub>	EC			
<b>Regal Black</b> (n = 41)								
16-084-04	24-Mar-16	24	0.02	0.69	28.34	29.05	2	98
16-098-03	7-Apr-16	22	-0.05	0.48	18.63	19.06	2	98
16-098-04	7-Apr-16	23	0.43	0.91	23.89	25.23	5	95
16-097-04	6-Apr-16	19	0.44	0.48	20.02	20.94	4	96
16-098-06	7-Apr-16	18	0.15	0.49	19.05	19.69	3	97
17-052-07	21-Feb-17	21	0.17	0.50	18.42	19.09	4	96
17-053-03	22-Feb-17	16	0.14	0.76	13.24	14.14	6	94
17-240-06	28-Aug-17	18	0.27	0.59	15.12	15.98	5	95
17-243-03	31-Aug-17	20	0.00	0.42	20.22	20.64	2	98
17-243-04	31-Aug-17	24	0.14	0.20	18.79	19.13	2	98
15-117-07	27-Apr-15	30	0.22	0.95	27.46	28.63	4	96
16-094-06	3-Apr-16	32	0.80	0.76	38.23	39.79	4	96
16-095-04	4-Apr-16	27	0.39	0.57	26.11	27.07	4	96
16-099-06	8-Apr-16	27	0.03	0.87	24.68	25.58	4	96
16-099-07	8-Apr-16	26	0.14	0.95	25.37	26.46	4	96
17-052-07	21-Feb-17	25	0.12	0.92	23.47	24.51	4	96
15-104-08	14-Apr-15	52	0.00	0.85	47.21	48.06	2	98
16-095-07	4-Apr-16	47	0.30	1.18	48.19	49.67	3	97
16-097-05	6-Apr-16	43	0.32	1.03	39.78	41.13	3	97
16-098-08	7-Apr-16	50	0.12	0.67	47.38	48.17	2	98
17-052-05	21-Feb-17	53	0.90	1.74	44.31	46.95	6	94
17-052-06	21-Feb-17	42	0.22	1.37	35.51	37.10	4	96
17-241-07	29-Aug-17	44	0.52	1.51	38.78	40.81	5	95
17-241-08	29-Aug-17	49	0.80	0.89	40.80	42.49	4	96
17-243-06	31-Aug-17	43	0.00	0.53	38.07	38.60	1	99

15-117-10	27-Apr-15	71	0.50	1.59	65.55	67.64	3	97	95
16-098-05	7-Apr-16	61	0.18	1.17	64.91	66.26	2	98	109
16-099-03	8-Apr-16	71	0.00	0.56	64.60	65.16	1	99	92
16-099-04	8-Apr-16	63	0.00	1.36	54.53	55.89	2	98	89
17-052-09	21-Feb-17	83	0.83	2.08	76.60	79.51	4	96	96
17-243-05	21-Feb-17	74	0.67	1.99	63.36	66.02	4	96	89
17-243-07	31-Aug-17	68	0.00	1.14	57.82	58.96	2	98	87
17-243-09	31-Aug-17	71	0.24	1.49	60.34	62.07	3	97	88
15-117-04	27-Apr-15	134	0.00	0.61	123.52	124.13	0	100	93
16-098-07	7-Apr-16	107	0.64	0.42	99.88	100.94	1	99	94
17-240-03	28-Aug-17	95	0.85	2.30	85.17	88.32	4	96	93
17-241-02	29-Aug-17	101	0.83	2.23	88.23	91.29	3	97	90
17-241-06	29-Aug-17	93	0.43	1.24	82.44	84.11	2	98	91
17-240-05	28-Aug-17	116	0.86	2.85	103.57	107.28	3	97	92
17-243-10	31-Aug-17	123	0.11	2.06	109.73	111.90	2	98	91
17-244-02	1-Sep-17	122	0.63	2.11	108.41	111.15	2	98	91
					<b>mean</b>	<b>3</b>	<b>97</b>	<b>96</b>	
					<b>s.d.</b>	<b>1</b>	<b>1</b>	<b>9</b>	
<b>C1150</b>	(n = 24)								
06-195-07	14-Jul-06	4	0.05	0.05	3.17	3.26	3	97	81
06-195-09	14-Jul-06	7	0.23	0.00	6.35	6.57	3	97	94
06-195-10	14-Jul-06	10	0.48	0.18	8.91	9.57	7	93	96
06-198-03	17-Jul-06	18	0.12	0.09	18.18	18.39	1	99	102
06-198-04	17-Jul-06	25	0.32	0.42	23.22	23.96	3	97	96
06-198-05	17-Jul-06	42	0.02	0.32	39.75	40.08	1	99	95
06-198-06	17-Jul-06	34	0.48	0.42	32.94	33.84	3	97	100
06-198-07	17-Jul-06	15	0.26	0.41	14.45	15.11	4	96	101
13-225-03	13-Aug-13	25	0.00	0.00	20.29	20.29	0	100	80
13-225-04	13-Aug-13	89	0.28	0.00	91.34	91.62	0	100	102
13-225-05	13-Aug-13	30	0.00	0.00	27.50	27.50	0	100	93
13-225-06	13-Aug-13	46	0.00	0.00	38.35	38.35	0	100	84
13-226-03	14-Aug-13	10	0.05	0.01	7.33	7.39	1	99	78
13-226-04	14-Aug-13	79	0.06	0.00	68.51	68.57	0	100	87
13-226-05	14-Aug-13	14	0.05	0.00	13.73	13.78	0	100	98

13-226-06	14-Aug-13	17	0.11	0.00	20.16	20.27	1	99	116
13-226-07	14-Aug-13	49	0.16	0.03	49.37	49.56	0	100	101
15-122-09	2-May-15	72	0.05	0.00	69.62	69.67	0	100	97
15-122-07	2-May-15	71	0.19	0.00	70.79	70.98	0	100	100
15-122-08	2-May-15	104	0.00	0.00	97.78	97.78	0	100	94
15-123-03	3-May-15	22	0.13	0.00	29.38	29.51	0	100	134
15-123-04	3-May-15	71	0.00	0.00	76.06	76.06	0	100	107
15-123-05	3-May-15	27	0.32	0.00	25.96	26.28	1	99	97
15-123-06	3-May-15	59	0.11	0.15	66.40	66.66	0	99	113
					<b>mean</b>		<b>1</b>	<b>99</b>	<b>98</b>
					<b>s.d.</b>		<b>2</b>	<b>2</b>	<b>12</b>
<b>Sucrose</b>	(n = 117)								
13-332-02	28-Nov-13	20	19.76	0.35	0.00	20.11	100	0	101
13-332-03	28-Nov-13	20	19.77	0.48	0.02	20.27	100	0	101
13-333-02	28-Nov-13	20	19.46	0.44	0.00	19.90	100	0	100
13-332-08	28-Nov-13	40	37.50	1.00	0.00	38.50	100	0	96
13-332-10	28-Nov-13	40	38.77	0.98	0.00	39.75	100	0	99
13-333-03	29-Nov-13	40	39.51	1.11	0.01	40.63	100	0	102
13-333-05	29-Nov-13	80	75.63	1.73	0.22	77.58	100	0	97
13-333-08	29-Nov-13	80	74.25	2.14	0.07	76.46	100	0	96
13-333-07	29-Nov-13	80	76.43	2.05	0.07	78.55	100	0	98
14-129-02	9-May-14	20	19.39	0.29	0.06	19.74	100	0	99
14-129-03	9-May-14	20	19.33	0.16	0.05	19.54	100	0	98
14-132-02	12-May-14	20	19.71	0.00	0.00	19.71	100	0	99
14-133-03	13-May-14	40	39.16	0.66	0.60	40.42	99	1	101
14-133-04	13-May-14	40	39.67	0.53	0.10	40.30	100	0	101
14-134-02	14-May-14	40	39.44	0.31	0.11	39.86	100	0	100
14-134-03	14-May-14	80	80.11	0.80	0.10	81.01	100	0	101
14-134-04	14-May-14	80	79.39	1.01	0.36	80.76	100	0	101
14-134-05	14-May-14	80	78.49	1.86	1.46	81.81	98	2	102
14-231-02	19-Aug-14	20	19.03	0.28	0.12	19.43	99	1	97
14-234-02	22-Aug-14	20	19.20	0.50	0.13	19.83	99	1	99
14-235-02	23-Aug-14	20	19.06	0.55	0.00	19.61	100	0	98
14-233-05	21-Aug-14	40	38.76	0.99	0.20	39.95	99	1	100

14-233-06	21-Aug-14	40	38.22	0.00	0.00	38.22	100	0	96
14-233-07	21-Aug-14	40	38.32	0.04	0.00	38.36	100	0	96
14-235-08	23-Aug-14	80	78.25	1.44	0.18	79.87	100	0	100
14-235-09	23-Aug-14	80	79.46	0.27	0.00	79.73	100	0	100
14-238-04	26-Aug-14	80	76.15	1.47	0.38	78.00	100	0	98
15-015-03	15-Jan-15	20	18.67	1.22	0.10	19.99	99	1	100
15-015-04	15-Jan-15	20	18.65	1.51	0.18	20.34	99	1	102
15-019-02	19-Jan-15	20	18.95	1.01	0.01	19.97	100	0	100
15-019-03	19-Jan-15	40	35.12	2.62	1.07	38.81	97	3	97
15-020-02	20-Jan-15	40	36.63	1.84	0.17	38.64	100	0	97
15-020-05	20-Jan-15	40	37.43	2.43	0.29	40.15	99	1	100
15-020-06	20-Jan-15	80	75.34	3.27	0.87	79.48	99	1	99
15-020-07	20-Jan-15	80	76.30	3.42	0.92	80.64	99	1	101
15-020-08	20-Jan-15	80	76.65	2.85	0.72	80.22	99	1	100
15-097-03	10-Apr-15	20	19.79	0.41	0.00	20.20	100	0	101
15-114-02	27-Apr-15	20	17.15	2.41	0.12	19.68	99	1	98
15-108-02	21-Apr-15	20	18.62	1.28	0.00	19.90	100	0	100
15-097-04	10-Apr-15	40	39.35	0.85	0.02	40.22	100	0	101
15-097-05	10-Apr-15	40	38.90	1.80	1.02	41.72	98	2	104
15-097-06	10-Apr-15	40	38.59	1.75	0.88	41.22	98	2	103
15-108-04	21-Apr-15	80	76.10	4.20	0.23	80.53	100	0	101
15-108-03	21-Apr-15	80	76.47	4.13	0.31	80.91	100	0	101
15-108-06	21-Apr-15	80	74.94	4.89	0.70	80.53	99	1	101
15-280-03	8-Oct-15	20	17.56	2.64	0.04	20.24	100	0	101
15-280-04	8-Oct-15	20	17.34	2.95	0.05	20.34	100	0	102
15-280-05	8-Oct-15	20	16.99	3.00	0.00	19.99	100	0	100
15-287-02	14-Oct-15	40	34.13	4.64	0.13	38.90	100	0	97
15-287-04	14-Oct-15	40	34.72	4.81	0.15	39.68	100	0	99
15-288-03	15-Oct-15	40	33.67	4.98	0.17	38.82	100	0	97
15-292-03	19-Oct-15	80	70.58	6.94	1.31	78.83	98	2	99
15-292-04	19-Oct-15	80	69.29	7.36	1.53	78.18	98	2	98
15-292-05	19-Oct-15	80	69.29	7.23	1.47	77.99	98	2	97
16-026-03	26-Jan-16	20	17.74	2.70	0.02	20.46	100	0	102
16-026-05	26-Jan-16	20	16.85	3.37	0.12	20.34	99	1	102

16-027-05	27-Jan-16	20	16.68	3.24	0.10	20.02	100	0	100
16-026-06	26-Jan-16	40	34.15	4.79	0.18	39.12	100	0	98
16-027-04	27-Jan-16	40	33.69	4.98	0.51	39.18	99	1	98
16-027-06	27-Jan-16	40	33.14	5.39	0.75	39.28	98	2	98
16-027-07	27-Jan-16	80	69.99	7.15	2.28	79.42	97	3	99
16-028-03	28-Jan-16	80	71.40	7.34	1.98	80.72	98	2	101
16-028-04	28-Jan-16	80	71.87	7.06	1.91	80.84	98	2	101
16-243-03	30-Aug-16	20	16.69	3.24	0.65	20.58	97	3	103
16-243-04	30-Aug-16	20	17.35	3.35	0.07	20.77	100	0	104
16-244-02	31-Aug-16	20	16.80	2.92	0.85	20.57	96	4	103
16-244-05	31-Aug-16	40	35.61	3.87	1.26	40.74	97	3	102
16-244-06	31-Aug-16	40	35.76	3.87	1.29	40.92	97	3	102
16-244-07	31-Aug-16	40	35.81	4.20	1.85	41.86	96	4	105
16-250-02	6-Sep-16	80	77.54	3.94	1.34	82.82	98	2	104
16-250-03	6-Sep-16	80	77.77	3.81	1.26	82.84	98	2	104
16-250-04	6-Sep-16	80	77.95	3.81	1.25	83.01	98	2	104
17-038-04	7-Feb-17	20	14.57	4.14	0.93	19.64	95	5	98
17-039-02	8-Feb-17	20	14.99	3.88	0.84	19.71	96	4	99
17-039-03	8-Feb-17	20	14.74	4.31	0.79	19.84	96	4	99
17-039-04	8-Feb-17	40	32.68	5.47	1.20	39.35	97	3	98
17-039-05	8-Feb-17	40	34.09	5.70	1.00	40.79	98	2	102
17-039-06	8-Feb-17	40	33.22	5.89	2.47	41.58	94	6	104
17-041-02	10-Feb-17	80	74.47	7.17	1.59	83.23	98	2	104
17-041-03	10-Feb-17	80	73.71	5.02	1.61	80.34	98	2	100
17-041-05	10-Feb-17	80	70.96	8.04	2.31	81.31	97	3	102
18-037-03	6-Feb-18	20	20.31	0.00	0.21	20.52	99	1	103
18-032-04	1-Feb-18	20	20.06	0.00	0.11	20.17	99	1	101
18-036-03	5-Feb-18	20	20.01	0.00	0.16	20.17	99	1	101
18-033-06	2-Feb-18	40	37.87	1.66	1.71	41.24	96	4	103
18-037-04	6-Feb-18	40	39.36	1.17	1.39	41.92	97	3	105
18-037-08	6-Feb-18	40	39.02	1.30	1.58	41.90	96	4	105
18-037-09	6-Feb-18	80	73.37	2.92	2.15	78.44	97	3	98
18-037-10	6-Feb-18	80	74.15	3.26	2.33	79.74	97	3	100
18-037-11	6-Feb-18	80	73.89	2.90	2.07	78.86	97	3	99

18-129-02	9-May-18	20	19.45	0.37	0.03	19.85	100	0	99
18-129-03	9-May-18	20	19.81	0.35	0.07	20.23	100	0	101
18-129-04	9-May-18	20	20.06	0.59	0.14	20.79	99	1	104
18-129-05	9-May-18	40	38.26	1.72	1.19	41.17	97	3	103
18-129-06	9-May-18	40	40.03	1.37	0.79	42.19	98	2	105
18-129-07	9-May-18	40	38.42	1.79	1.21	41.42	97	3	104
18-130-02	10-May-18	80	80.93	0.95	0.58	82.46	99	1	103
18-130-03	10-May-18	80	81.34	1.02	0.28	82.64	100	0	103
18-131-08	11-May-18	80	81.52	1.86	0.72	84.10	99	1	105
18-297-02	24-Oct-18	20	19.44	0.45	0.03	19.92	100	0	100
18-302-03	29-Oct-18	20	19.09	0.84	0.36	20.29	98	2	101
18-298-06	25-Oct-18	20	19.17	0.71	0.13	20.01	99	1	100
18-302-06	29-Oct-18	40	39.37	0.89	0.17	40.43	100	0	101
18-298-07	25-Oct-18	40	39.68	0.42	0.29	40.39	99	1	101
18-309-08	5-Nov-18	40	41.22	0.25	0.00	41.47	100	0	104
18-309-11	5-Nov-18	80	78.46	0.81	0.20	79.47	100	0	99
18-309-14	5-Nov-18	80	78.26	1.56	0.15	79.97	100	0	100
18-310-03	6-Nov-18	80	82.01	1.75	0.50	84.26	99	1	105
18-355-02	21-Dec-18	20	22.04	0.99	0.24	23.27	99	1	116
18-355-03	21-Dec-18	20	21.48	1.11	0.15	22.74	99	1	114
18-355-04	21-Dec-18	20	21.17	1.31	0.26	22.74	99	1	114
18-361-04	27-Dec-18	40	42.02	1.29	0.13	43.44	100	0	109
18-361-05	27-Dec-18	40	41.56	0.93	0.00	42.49	100	0	106
18-361-06	27-Dec-18	40	41.06	1.85	0.23	43.14	99	1	108
18-361-07	27-Dec-18	80	85.76	2.27	0.75	88.78	99	1	111
18-361-08	27-Dec-18	80	86.49	2.48	0.78	89.75	99	1	112
18-361-09	27-Dec-18	80	85.98	2.63	0.61	89.22	99	1	112
					<b>mean</b>	<b>99</b>	<b>1</b>	<b>101</b>	
					<b>s.d.</b>	<b>1</b>	<b>1</b>	<b>4</b>	
<b>Adipic Acid</b> (n = 5)									
15-062-06	3-Mar-15	34	13.67	0.09	0.00	13.76	100	0	40
15-062-05	3-Mar-15	102	47.47	0.00	0.00	47.47	100	0	47
15-100-02	13-Apr-15	n/a	5.25	0.00	0.05	5.30	99	1	n/a
19-137-05	17-May-19	253	120.68	1.05	0.07	121.80	100	0	48

19-137-06	17-May-19	28	10.62	0.00	0.00	10.62	100	0	38
						<b>mean</b>	<b>100</b>	<b>0</b>	<b>43</b>
						<b>s.d.</b>	<b>0</b>	<b>0</b>	<b>5</b>
<b>Rice Char</b>	<b>(n = 6)</b>								
18-158-05	7-Jun-18	112	4.27	3.25	49.54	57.06	13	87	51
18-164-05	13-Jun-18	212	8.73	6.22	96.87	111.82	13	87	53
18-165-06	14-Jun-18	79	2.96	2.86	35.46	41.28	14	86	52
18-169-04	18-Jun-18	71	2.76	2.70	30.18	35.64	15	85	51
18-172-05	21-Jun-18	150	5.74	4.28	70.40	80.42	12	88	54
18-176-06	25-Jun-18	121	4.83	4.67	56.43	65.93	14	86	54
						<b>mean</b>	<b>14</b>	<b>86</b>	<b>52</b>
						<b>s.d.</b>	<b>1</b>	<b>1</b>	<b>1</b>
<b>SRM-1649a</b>	<b>(n = 6)</b>								
04-271-04	27-Sep-04	690	29.94	9.65	36.46	76.05	52.1	47.9	16.5
04-322-10	17-Nov-04	490	25.82	7.18	30.41	63.41	52.0	48.0	19.4
04-322-12	17-Nov-04	880	40.28	11.25	47.71	99.24	51.9	48.1	16.9
05-046-02	15-Feb-05	1101	51.66	16.59	67.16	135.41	50.4	49.6	18.5
05-046-03	15-Feb-05	441	21.06	6.41	25.35	52.82	52.0	48.0	18.0
05-046-04	15-Feb-05	855	40.33	12.37	51.22	103.92	50.7	49.3	18.2
						<b>mean</b>	<b>51.5</b>	<b>48.5</b>	<b>17.9</b>
						<b>s.d.</b>	<b>0.8</b>	<b>0.8</b>	<b>1.1</b>

<sup>a</sup>Loaded mass are the weighed mass (for Regal black, C1150, Adipic acid, Rice char and SRM-1649a) or injected mass (sucrose) on the filter.

**Table S2.** Radiocarbon content of bulk reference materials, expressed as fraction modern carbon (FM) with and without background correction. CO<sub>2</sub> isolation and <sup>14</sup>C/<sup>12</sup>C analysis were carried out at KCCAMS, UCI (the method is described in Table 2).

UCI AMS #	Size μg C	Corrected FM		Uncorrected FM	
		±	915	±	915
<b>Sucrose</b>					
150230	735	1.0597	0.0021	1.0597	0.0021
150231	769	1.0575	0.0017	1.0574	0.0017
<b>Adipic Acid</b>					
			920		
123428	876	0.0002	0.0005	0.0020	0.0001
123430	851	0.0001	0.0005	0.0019	0.0001
123431	934	-0.0001	0.0005	0.0016	0.0001
123432	1053	-0.0003	0.0005	0.0015	0.0001 <sup>25</sup>
123433	740	-0.0001	0.0005	0.0016	0.0001
<b>Regal Black</b>					
150228	717	0.0004	0.0005	0.0019	0.0001
150229	752	-0.0005	0.0005	0.0011	0.0000 <sup>30</sup>
<b>C1150</b>					
150232	88	0.0026	0.0005	0.0042	0.0001
150233	64	0.0035	0.0005	0.0050	0.0002
150234	560	0.0019	0.0005	0.0035	0.0001 <sup>35</sup>
<b>Rice Char</b>					
123434	924	1.0683	0.0023	1.0683	0.0023
123435	913	1.0670	0.0018	1.0670	0.0018
123436	961	1.0673	0.0019	1.0672	0.0019

**Table S3.** Stable isotopic composition ( $^{13}\text{C}/^{12}\text{C}$ ) of OC and EC fractions or bulk materials.  $\text{CO}_2$  isolation and  $^{13}\text{C}/^{12}\text{C}$  analysis were carried out at the CAIR lab, CRD, ASTD/ECCC (the method is described in Table 2).

Reference	Lab ID	Date	Fraction	Loaded mass on filter μg or μg C <sup>a</sup>	$\delta^{13}\text{C}_{\text{VPDB}}$ ‰
<b>Regal Black</b> (n = 5)	16-036-04	5-Feb-16	EC	16	-27.67
	16-036-05	5-Feb-16	EC	27	-27.49
	16-036-06	5-Feb-16	EC	22	-27.67
	16-036-08	5-Feb-16	EC	59	-27.62
	16-036-09	5-Feb-16	EC	68	-27.57
				<b>mean</b>	<b>-27.61</b>
				<b>s.d.</b>	<b>0.08</b>
<b>C1150</b> (n = 5)	13-013-05	13-Jan-13	EC	50	-23.01
	13-013-07	13-Jan-13	EC	22	-23.16
	13-013-08	13-Jan-13	EC	48	-22.96
	16-036-06	5-Feb-16	EC	30	-23.14
	16-036-07	5-Feb-16	EC	46	-23.05
				<b>mean</b>	<b>-23.06</b>
				<b>s.d.</b>	<b>0.08</b>
<b>Sucrose<sup>b</sup></b> (n = 9)	15-146-07	26-May-15	OC	20	-12.08
	15-148-03	27-May-15	OC	20	-12.40
	15-148-04	27-May-15	OC	20	-12.31
		5-Oct-17	OC	20	-12.44
		18-Apr-18	OC	20	-12.04
		18-Apr-18	OC	20	-12.30
		26-Feb-19	OC	20	-12.21
		26-Feb-19	OC	20	-12.16
		26-Feb-19	OC	20	-12.04
					<b>mean</b>
					<b>-12.22</b>
					<b>s.d.</b>
					<b>0.15</b>
<b>Rice Char</b> (n = 1)	04-328-06	23-Nov-04	OC	n/m	-24.42
	04-328-07	23-Nov-04	PyOC	n/m	-26.67
	04-328-05	23-Nov-04	EC	n/m	-26.94

		fraction weighted	TC	160	<b>-26.74</b>
<b>SRM-1649a</b>					
(n = 2)	04-330-03	25-Nov-04	OC	n/m	-26.38
	04-338-08	3-Dec-04	OC	n/m	-26.29
	04-330-05	25-Nov-04	PyOC	n/m	-25.51
	04-338-07	3-Dec-04	PyOC	n/m	-25.66
	04-330-06	25-Nov-04	EC	n/m	-25.56
	04-338-09	3-Dec-04	EC	n/m	-25.43
	fraction <sup>c</sup> weighted		TC	~ 600	<b>-25.84 ± 0.07</b>

940 <sup>a</sup>Sucrose was loaded as a solution (µg C), Regal Black, C1150, Rice char, and SRM-1649a as a powder (µg dry mass); <sup>b</sup> $\delta^{13}\text{C}_{\text{VPDB}}$  of bulk material (sucrose) via off-line method:  $-12.0 \pm 0.2\text{‰}$  (Satoshi, 2008); <sup>c</sup>Mean fraction (of two measurements) weighted isotopic composition of TC; n/m = not measured.

**Table S4.** Stable isotopic compositions of  $^{13}\text{C}/^{12}\text{C}$  in OC and EC fractions from mixtures of reference materials. OC and EC fractions were isolated with the ECT9 protocol (Huang et al., 2006), purified in a vacuum system and analyzed on a MAT253 (Huang et al., 2013) at the CAIR lab, CRD, ASTD/ECCC.

Reference mate	Lab ID	Date	Initial mass		Measured fraction	$\delta^{13}\text{C}_{\text{VPDB}}$ (‰)
			Sucrose	Regal Black		
			µg C	µg		
<b>Regal Black</b>	15-148-08	28-May-15	10	22	EC	-27.49
	15-148-05	28-May-15	15	26	EC	-27.73
	15-149-07	29-May-15	20	50.4	EC	-27.34
	15-148-09	28-May-15	30	66	EC	-27.32
	16-224-04	11-Aug-16	20	57	EC	-27.31
	16-224-07	11-Aug-16	20	53	EC	-27.27
	16-224-08	11-Aug-16	20	58	EC	-27.37
	16-225-07	12-Aug-16	10	20	EC	-27.57
	17-248-08	30-Aug-17	20	53	EC	-27.47
				<b>mean</b>	<b>-27.43</b>	
				<b>s.d.</b>	<b>0.15</b>	
<b>Sucrose</b>	15-149-04	29-May-15	10	22	OC	-12.82
	15-148-06	28-May-15	15	26	OC	-12.54
	15-149-05	29-May-15	20	50.4	OC	-12.54
	15-149-06	29-May-15	30	66	OC	-12.29
	16-224-05	11-Aug-16	20	57	OC	-13.04
	16-224-06	11-Aug-16	20	53	OC	-12.36
	16-225-03	12-Aug-16	20	58	OC	-12.72
	16-225-04	12-Aug-16	10	20	OC	-12.86
	17-242-06	30-Aug-17	20	53	OC	-12.34
				<b>mean</b>	<b>-12.61</b>	
				<b>s.d.</b>	<b>0.26</b>	

945 **Table S5.** Calculated stable isotopic composition ( $^{13}\text{C}/^{12}\text{C}$ ) in a two-end-member-mixing system with endmember #1 being Sucrose ( $\delta^{13}\text{C}_{\text{VPDB}} = -12.22\text{\textperthousand}$ ) and end member #2 being Regal black ( $\delta^{13}\text{C}_{\text{VPDB}} = -27.61\text{\textperthousand}$ ) and where endmember #1 is mixed into endmember#2.

$\delta^{13}\text{C}_{\text{VPDB}}$ of pure endmember	<i>fraction of sucrose in mixture</i> (Sucrose + Regal black)	$\delta^{13}\text{C}_{\text{VPDB}}$ of the mixture calculated
Sucrose	Regal black	%
%		%
-12.22	-27.61	0
		-27.610
		1
		-27.456
		2
		-27.302
		3
		-27.148
		4
		-26.994
		5
		-26.841
		10
		-26.071
		20
		-24.532
		30
		-22.993
		40
		-21.454
		50
		-19.915
		60
		-18.376
		70
		-16.837
		80
		-15.298
		90
		-13.759
		91
		-13.605
		92
		-13.451
		93
		-13.297
		94
		-13.143
		95
		-12.990
		96
		-12.836
		97
		-12.682
		98
		-12.528
		99
		-12.374
		100
		-12.220

**Table S6.** Radiocarbon content, expressed as fraction modern carbon (FM), of total (TC), organic (OC), and elemental (EC) carbon fractions with and without background correction following Santos et al. (2010). OC and EC fractions were isolated with the ECT9 protocol (Huang et al., 2006) from pure reference materials (into the form of  $\text{CO}_2$ ), then purified cryogenically and sealed in ampoules at the CAIR lab, ECCC.  $\text{CO}_2$  is reduced to graphite (Santos et al., 2007b, 2007a) and analyzed at the KCCAMS facility.

UCIAMS#	Fraction	Mass after	Mass	Corrected FM		Uncorrected FM	
		ECT9	μgC	±	±	±	±
<b>Adipicacid</b>							
153279	TC	10	14	-0.0050	0.0367	0.0593	0.0010
153280	TC	17	16	-0.0116	0.0325	0.0465	0.0009
153281	TC	23	29	-0.0043	0.0165	0.0268	0.0005
153282	TC	37	37	-0.0102	0.0125	0.0140	0.0006
mean				-0.0078			
s.d.				0.0037			
<b>Sucrose</b>							
153283	TC	5	7	1.0041	0.0885	0.8766	0.0101
153284	TC	5	7	1.0031	0.0878	0.8759	0.0051
153285	TC	5	7	1.0346	0.0938	0.8960	0.0064
153286	TC	10	11	1.0529	0.0516	0.9652	0.0045
153287	TC	10	11	1.0360	0.0511	0.9510	0.0070
153288	TC	10	12	1.0571	0.0510	0.9702	0.0056
153289	TC	20	21	1.0477	0.0265	1.0006	0.0069
153290	TC	20	21	1.0429	0.0257	0.9971	0.0058
153291	TC	20	21	1.0470	0.0262	1.0000	0.0056
153292	TC	40	41	1.0405	0.0127	1.0170	0.0034
153293	TC	40	38	1.0543	0.0139	1.0282	0.0034
153294	TC	40	42	1.0509	0.0125	1.0272	0.0026
153295	OC	20	20	1.0844	0.0290	1.0305	0.0041
mean				1.0427			
s.d.				0.0213			
<b>C1150</b>							
153303	TC	7	10	0.0310	0.0535	0.1154	0.0020
153304	TC	16	23	0.0278	0.0205	0.0644	0.0012
153305	TC	34	36	-0.0012	0.0131	0.0237	0.0006
153306	TC	45	55	0.0041	0.0083	0.0201	0.0003

153307	EC	32	33	-0.0072	0.0144	0.0202	0.0004
mean				0.0109			
s.d.				0.0174			
<b>RegalBlack</b>							
153308	TC	16	23	0.0161	0.0209	0.0540	0.0008
153309	TC	47	53	-0.0008	0.0087	0.0160	0.0004
153310	EC	28	41	-0.0057	0.0112	0.0159	0.0004
mean				0.0032			
s.d.				0.0114			
<b>Ricechar</b>							
153299	TC	6	7	0.9383	0.0830	0.8272	0.0097
153300	TC	12	15	1.0463	0.0390	0.9784	0.0057
153301	TC	24	22	1.0823	0.0254	1.0348	0.0046
153302	EC	13	15	1.0621	0.0383	0.9940	0.0046
mean				1.0323			
s.d.				0.0643			
<b>OxalicacidII<sup>a</sup></b>							
153316	TC	n/a	7	1.3141	0.0398	1.2411	0.0203
153315	TC	n/a	17	1.3365	0.0137	1.3080	0.0063
153314	TC	n/a	45	1.3342	0.0051	1.3235	0.0027
mean				1.3283			
s.d.				0.0123			
<b>Adipicacid<sup>a</sup></b>							
153318	TC	n/a	6	-0.0020	0.0313	0.0544	0.0031
153317	TC	n/a	16	-0.0016	0.0115	0.0205	0.0011
153278	TC	n/a	56	-0.0014	0.0033	0.0051	0.0003
mean				-0.0017			
s.d.				0.0003			

<sup>a</sup>Reference standards that underwent combustion and graphitization process only for blank determination at KCCAMS (without ECT9); n/a. = not applicable

**Table S7.** Radiocarbon content, expressed as fraction modern carbon (FM), of total (TC), organic (OC), and elemental (EC) carbon fractions with and without background correction following Santos et al. (2010). OC and EC fractions were isolated with the ECT9 protocol (Huang et al., 2006) from mixtures of reference materials (into the form of CO<sub>2</sub>), then purified cryogenically and sealed in ampoules at ECCC. CO<sub>2</sub> is reduced to graphite (Santos et al., 2007b, 2007a) and analyzed at KCCAMS facility.

UCI AMS #	Fraction measured	Initial loaded mass		Mass after ECT9	Mass at KCCAMS	Corrected FM		Uncorrected FM	
		μg C	μg			μg C	±	±	
<b>Sucrose + Regal black</b>									
159800	OC	5	10	5	6	1.0568	0.0648	0.9738	0.0107
159802	OC	10	21	11	10	1.0542	0.0337	1.0057	0.0049
159804	OC	15	29	16	15	1.0629	0.0216	1.0298	0.0037
159806	OC	20	39	21	20	1.0436	0.0156	1.0201	0.0034
159808	OC	30	63	32	29	1.0563	0.0107	1.0395	0.0025
<u>mean</u>		<u>1.0548</u>		<u>0.0070</u>					
<u>s.d.</u>									
159801	EC	5	10	10	11	-0.0361	-0.0502	0.0535	0.0014
159803	EC	10	21	20	19	-0.0189	-0.0270	0.0317	0.0007
159805	EC	15	29	28	36	-0.0091	-0.0136	0.0172	0.0005
159807	EC	20	39	38	44	0.0014	0.0110	0.0226	0.0004
159809	EC	30	63	61	56	0.0019	0.0085	0.0186	0.0003
<u>mean</u>		<u>-0.0122</u>		<u>0.0159</u>					
<u>s.d.</u>									
<b>Adipic acid + Bulk rice char<sup>a</sup></b>									
159822	OC	5	11	6	6	0.1009	0.0856	0.2279	0.0027
159824	OC	10	22	12	11	0.0759	0.0450	0.1516	0.0021
159826	OC	15	35	18	17	0.1078	0.0278	0.1558	0.0013
159828	OC	20	44	23	22	0.1072	0.0204	0.1432	0.0014
159830	OC	25	51	29	23	0.1552	0.0185	0.1868	0.0011
159832	OC	30	60	34	32	0.1013	0.0138	0.1263	0.0009
<u>mean</u>		<u>0.1081</u>		<u>0.0250</u>					
<u>s.d.</u>									
159823	EC	5	11	5	5	1.1063	0.0887	0.9903	0.0063
159825	EC	10	22	10	8	1.0981	0.0486	1.0263	0.0052
159827	EC	15	35	16	14	1.0559	0.0231	1.0211	0.0034

159829	EC	20	44	20	17	1.0619	0.0190	1.0328	0.0040
159831	EC	25	51	23	22	1.0625	0.0143	1.0400	0.0027
159833	EC	30	60	27	24	1.0633	0.0131	1.0426	0.0028
<u>mean</u>						<u>1.0747</u>			
<u>s.d.</u>						<u>0.0216</u>			
<b>Adipic acid + Rice char_EC<sup>b</sup></b>		Adipic acid	Rice char(EC						
159810	OC	5	13	5	6	-0.0605	-0.1166	0.1212	0.0032
159812	OC	10	19	10	10	-0.0324	-0.0558	0.0655	0.0015
159814	OC	15	34	15	15	-0.0075	-0.0345	0.0556	0.0008
159816	OC	20	38	20	20	0.0107	0.0248	0.0568	0.0011
159818	OC	25	49	25	25	-0.0009	-0.0198	0.0366	0.0005
159820	OC	30	60	30	29	0.0103	0.0168	0.0421	0.0006
<u>mean</u>						<u>-0.0134</u>			
<u>s.d.</u>						<u>0.0280</u>			
159811	EC	5	13	6	5	1.0926	0.0931	0.9755	0.0094
159813	EC	10	19	8	7	1.0702	0.0506	0.9997	0.0058
159815	EC	15	34	15	16	1.0709	0.0203	1.0392	0.0037
159817	EC	20	38	17	20	1.0726	0.0162	1.0471	0.0038
159819	EC	25	49	22	21	1.0749	0.0152	1.0505	0.0029
159821	EC	30	60	27	27	1.0723	0.0116	1.0535	0.0024
<u>mean</u>						<u>1.0756</u>			
<u>s.d.</u>						<u>0.0085</u>			

<sup>a</sup>The bulk rice char contains 52% of TC, on which 14% is OC and 86% EC, respectively; <sup>b</sup>Adipic acid was injected after the OC of rice char is removed through combustion at 870°C via ECT9. Thus, adipic acid was mixed only with rice char-EC, and the OC of the mixture is only from Adipic acid and EC of the mixture is only from Rice char.